INTERNATIONAL JOURNAL FOR NUMERICAL METHODS IN ENGINEERING
Int. J. Numer. Meth. Engng 2011; **85**:1705–1736
Published online 28 October 2010 in Wiley Online Library (wileyonlinelibrary.com). DOI: 10.1002/nme.3051

Finite element modelling of saturated porous media at finite strains under dynamic conditions with compressible constituents

A. Gajo[1,*,†] and R. Denzer[2]

[1]*Dipartimento di Ingegneria Meccanica e Strutturale, Università di Trento, Via Mesiano 77-38050 Povo, Trento, Italy*
[2]*Institute of Mechanics, Technical University of Dortmund, Leonhard-Euler-Strasse 5, D-44227 Dortmund, Germany*

SUMMARY

Two finite element formulations are proposed to analyse the dynamic conditions of saturated porous media at large strains with compressible solid and fluid constituents. Unlike similar works published in the literature, the proposed formulations are based on a recently proposed hyperelastic framework in which the compressibility of the solid and fluid constituents is fully taken into account when geometrical non-linear effects are relevant on both micro- and macroscales. The first formulation leads to a three-field finite element method (FEM), which is suitable for analysing high-frequency dynamic problems, whereas the second is a simplification of the first, leading to a two-field FEM, in which some inertial effects of the pore fluid are disregarded, hence the second formulation is suitable for studying low-frequency problems. A fully Lagrangian approach is considered, hence all terms are expressed with reference to the material setting; the balance equations for the pore fluid are also expressed in terms of the chemical potential and the mass flux of the pore fluid in order to take the compressibility of the fluid into account. To improve the numerical response in the case of wave propagation, a discontinuous Galerkin FEM in the time domain is applied to the three-field formulation. The results are compared with analytical and semi-analytical solutions, highlighting the different effects of the discontinuous Galerkin method on the longitudinal waves of the first and second kind.

Received 28 January 2010; Revised 26 August 2010; Accepted 26 August 2010

KEY WORDS: saturated porous media; compressible constituents; finite strains; dynamic behaviour; finite elements

1. INTRODUCTION

The analysis of the transient response of multiphase porous media is of interest in a number of applications, such as environmental problems, petroleum engineering, geophysics, geotechnical engineering, earthquake engineering, industrial processes and bio-engineering (e.g. Loix *et al.* [1] for articular cartilages). Most of these applications typically involve non-linear geometrical and material effects, as in the case of biological tissues, numerous industrial processes and geotechnical engineering (e.g. slope stability, consolidation of soft sediments).

Within the framework of geometrically linear theory and constant volume fractions, Biot [2–5] was the first to give a complete description of fluid-saturated, elastic isotropic porous media with compressible constituents, and to consider the harmonic wave propagation. Two apparently different approaches have since been used: mixture theories [6–8] and the so-called 'purely macroscale

*Correspondence to: A. Gajo, Dipartimento di Ingegneria Meccanica e Strutturale, Università di Trento, Via Mesiano 77, I-38050 Trento, Italy.
†E-mail: alessandro.gajo@ing.unitn.it

theories', in which the standard concepts of continuum mechanics are assumed to be relevant on a macroscale too [9–12]. The two formulations are related to each other, however, and the choice is only a matter of personal preference [13], in fact Schanz and Diebels [14] showed that the Biot and Bowen models coincide with each other in the case of linear theory.

For the small strain analysis of dynamic problems, Biot's theory provided the basis for a number of analytical (e.g. [15–19]) and numerical solutions based on the finite difference method (e.g. [15]) and the finite element method (FEM) with two or three unknown fields [16, 17, 20–22].

Large strain effects were first considered in the numerical solutions by Carter *et al.* [23] for the consolidation problem and by Prevost [24] for dynamic problems in fully saturated conditions. Since then, a number of finite strain numerical solutions have been proposed, within the framework of both mixture theory and purely macroscale theory, for analysing both saturated and unsaturated porous media, under isothermal and non-isothermal conditions, for dynamic and quasi-static loadings.

It is generally agreed that the assumption of incompressibility of the solid grains *immensely* simplifies the relationships [25], hence an interesting term of comparison between the various proposed solutions is whether the compressibility of the solid constituent has been considered or not. Most of the proposed numerical solutions for large strain analysis disregard the compressibility of the solid constituents [24, 26–36], while some numerical approaches have considered the solid constituent in a simplified way: Advani *et al.* [37] considered the *semilinear*, simplified approach (originally proposed by Boit [10], see also Gajo [38]) according to which the compressibility of the solid constituents is described by a geometrical linear theory (combined with the non-linear theory adopted for the solid skeleton), Lewis and Schrefler [39], Armero [40], Li *et al.* [41] and Callari & Armero [42] treated the compressibility of the constituents in a simplified manner by considering Biot's coefficients as constant (as in linear theory), Bluhm and de Boer [43] and Diebels [44] restricted their general, large-strain framework to the definition of effective stress proposed by Suklje [45] for small strains, Bernaud *et al.* [46] considered small elastic deformations (as opposed to the large plastic deformations) so that Biot's coefficients turn out to be constant, Larsson *et al.* [47] identified the solid constituent with the fibre bundles being wetted with resin in the processing of fibre composite materials and assumed that the solid constituent may become compact as a result of pore pressure and wetting alone, thus disregarding the role of the effective stress, and finally Borja [48] proposed a geometrically non-linear theoretical framework based on the current configuration, in which the definition of effective stress proposed by Nur and Byerlee [49] for small strains is recovered with non-constant coefficients. As a result, to the best of the Authors' knowledge, no numerical solution strictly considering the compressibility of the solid constituents at large strains has been proposed as yet.

It is worth adding that some of the earlier cited numerical solutions were based on the Jaumann stress rate in an updated Lagrangian approach (e.g. [24, 26]), which may lead to unphysical responses [50], whereas the most recent solutions are based on hyperelastic formulations.

The objective of this paper is to provide the finite element implementation for dynamic analyses of the hyperelastic framework recently proposed by Gajo [38] for saturated porous media with compressible constituents subjected to finite strains. This recent hyperelastic model fully takes into account all the non-linear terms, both in the solid skeleton and in the fluid and solid constituents. In particular, two finite element formulations are considered: the first consists of a three-field formulation suitable for high-frequency dynamic problems and the second consists of a two-field formulation, which is a simplification of the first in which *some* terms of the pore fluid inertial forces are disregarded. The second formulation, therefore, does not permit a reliable analysis of the highest frequency components, hence it is suitable for problems in which the frequency components are not excessively high for the range of permeability involved [51]. The two formulations are direct extensions to large strains of the corresponding formulations proposed for small strain analyses (which are known as $\boldsymbol{u}-\boldsymbol{w}-p$ and $\boldsymbol{u}-p$ formulations [21, 22]). It is worth adding that providing the range of applicability of the two-field formulation is no easy task, because the frequency content, the propagation length and the permeability are interrelated. In fact, the highest frequency components are the fastest, but they are also the most heavily damped (for a more detailed discussion on this topic, see [52]).

DOI: 10.1002/nme

The novelties of this work are the following:

- the compressibility of the solid and fluid constituents is fully taken into account when geometrical non-linear effects are relevant in both the constituents (i.e. at the microscale) and the solid skeleton (i.e. on the macroscale);
- the momentum and mass balance equations for the pore fluid are expressed in terms of the chemical potential and the mass flux of the pore fluid, in order to take the compressibility of the fluid into due account;
- a three-field formulation involving the chemical potential of pore fluid is proposed for dealing with high-frequency dynamic problems at large strains and is validated against analytical results;
- the three-field formulation is actually obtained from a four-field formulation, in which the nodal mass fluxes are deduced in a weak form from the nodal relative velocities of the pore fluid;
- a fully Lagrangian formulation is considered, so that all terms are expressed with reference to the material setting, leading to a reduction of the computational burden because many intermediate matrices remain constant during the loading history;
- to improve the numerical response of the proposed FEM in the case of a wave propagation, the discontinuous Galerkin FEM in the time domain is applied for the first time to a *realistic* wave propagation evaluated with a three-field formulation for saturated porous media (in fact, Chen *et al.* [53] only considered incompressible solid and fluid constituents and could consequently only analyse the propagation of one kind of longitudinal wave) and its effectiveness is considered for the longitudinal waves of the first and second kind.

It is finally worth adding that there is not just one possible weak form formulation of the same momentum and mass balance equations, but the one proposed in this work was found to work effectively.

The layout of the paper is as follows. For the sake of completeness, Sections 2 and 3 briefly recall the balance equations in the case of compressible fluid and solid constituents, in the spatial setting. The hyperelastic formulation proposed by Gajo [38] is recalled in Section 4, in terms of the first Piola–Kirchhoff stress tensor $\boldsymbol{S}$ and the chemical potential of pore fluid μ_w as stress-like quantities on the one hand, and the deformation gradient $\boldsymbol{F}$ and the variation of fluid mass content $\bar{m}_w$ as strain-like quantities on the other. In Section 5 the governing equations are expressed in two different weak forms, which enable the application of the FEM. In Section 6 the numerical results are compared with analytical and semi-analytical evaluations concerning both quasi-static and dynamic, one (1D)- and two-dimensional (2D) problems, and the effects induced by the compressibility of the solid constituents are shown.

Notation

Two tensorial products will be employed, which can be defined as follows:

$$(\boldsymbol{A}\otimes\boldsymbol{B})[\boldsymbol{C}]=(\boldsymbol{B}\bullet\boldsymbol{C})\boldsymbol{A},\quad (\boldsymbol{A}\overline{\underline{\otimes}}\boldsymbol{B})[\boldsymbol{C}]=\tfrac{1}{2}(\boldsymbol{A}\boldsymbol{C}\boldsymbol{B}^{\mathrm{T}}+\boldsymbol{A}\boldsymbol{C}^{\mathrm{T}}\boldsymbol{B}^{\mathrm{T}})$$

$$(\boldsymbol{A}\overline{\otimes}\boldsymbol{B})[\boldsymbol{C}]=\boldsymbol{A}\boldsymbol{C}\boldsymbol{B}^{\mathrm{T}}\quad\text{and}\quad(\boldsymbol{A}\underline{\otimes}\boldsymbol{B})[\boldsymbol{C}]=\boldsymbol{A}\boldsymbol{C}^{\mathrm{T}}\boldsymbol{B}^{\mathrm{T}}$$

for every second-order tensor $\boldsymbol{A}$, $\boldsymbol{B}$ and $\boldsymbol{C}$. The alternative index definition is given in the footnote.[‡] Moreover, let Grad$(\bullet)$ of an arbitrary quantity $(\bullet)$ denote the material gradient of the material description of the quantity $(\bullet)$, while grad$(\bullet)$ denotes the spatial gradient of the spatial description of $(\bullet)$. Equivalently, Div$(\bullet)$ and div$(\bullet)$ denote the material and spatial divergence of the material and spatial description of $(\bullet)$, respectively.

[‡]In index notation $(\boldsymbol{A}\otimes\boldsymbol{B})_{ijkl}=A_{ij}B_{kl}$, $(\boldsymbol{A}\overline{\underline{\otimes}}\boldsymbol{B})_{ijkl}=(A_{ik}B_{jl}+A_{il}B_{jk})/2$, $(\boldsymbol{A}\overline{\otimes}\boldsymbol{B})_{ijkl}=A_{ik}B_{jl}$, and $(\boldsymbol{A}\underline{\otimes}\boldsymbol{B})_{ijkl}=A_{il}B_{jk}$.

DOI: 10.1002/nme

2. BASIC GEOMETRY

Let $\boldsymbol{x}=\boldsymbol{\varphi}(\boldsymbol{X},t)$ denote the current position (with $\boldsymbol{x}\in\mathscr{B}$ in the current configuration $\mathscr{B}$) of the solid skeleton particle having the initial position $\boldsymbol{X}\in\mathscr{B}_0$ in the reference configuration $\mathscr{B}_0$. Then let $\boldsymbol{F}=\mathrm{Grad}\,\boldsymbol{\varphi}$, and $J=\det\boldsymbol{F}$ denote the deformation gradient and its Jacobian, respectively. Thus, the current infinitesimal volume $\mathrm{d}\Omega$ of the solid skeleton is related to its initial material volume $\mathrm{d}\Omega_0$, through $\mathrm{d}\Omega=J\,\mathrm{d}\Omega_0$.

The volume occupied by the pore fluid in the reference configuration is $n_0\mathrm{d}\Omega_0$, where n_0 is the initial porosity in the reference configuration; let n denote the current porosity. If ρ_w and ρ_{w0} denote the current and the initial density of the pore fluid, respectively, their ratio is $J_w=\rho_{w0}/\rho_w$.

In the infinitesimal solid volume $\mathrm{d}\Omega_0$, the initial pore fluid mass content equates to

$$\mathrm{d}\tilde{m}_{w0}=\rho_{w0}n_0\mathrm{d}\Omega_0 \tag{1}$$

while the current pore fluid mass content in $\mathrm{d}\Omega$ is

$$\mathrm{d}\tilde{m}_w=\rho_w n\mathrm{d}\Omega \tag{2}$$

which can be rewritten as

$$\mathrm{d}\tilde{m}_w=\rho_{w0}\frac{nJ}{J_w}\mathrm{d}\Omega_0 \tag{3}$$

Let m_{w0} and m_w denote the initial and the current fluid mass content, respectively, both evaluated per unit of solid volume in the reference configuration, namely $m_{w0}=\mathrm{d}\tilde{m}_{w0}/\mathrm{d}\Omega_0$ and $m_w=\mathrm{d}\tilde{m}_w/\mathrm{d}\Omega_0$. Then, from Equation (3), the ratio J_w results as

$$J_w=\rho_{w0}\frac{nJ}{m_w} \tag{4}$$

Finally, the variation in fluid mass content (coinciding with the exchanged mass of pore fluid) per unit volume of the undeformed solid skeleton, $\bar{m}_w$, is given by the difference between the current and the initial fluid mass content

$$\bar{m}_w=m_w-m_{w0}=\rho_w nJ-\rho_{w0}n_0 \tag{5}$$

Likewise, let ρ_{s0} and ρ_s denote the initial and the current density of the solid constituent, respectively, and let J_s denote their ratio

$$J_s=\rho_{s0}/\rho_s \tag{6}$$

Note that J_s represents the local ratio of the deformed to the undeformed volume of the solid constituent, namely $J_s=\mathrm{d}\Omega_s/\mathrm{d}\Omega_{s0}$, where $\mathrm{d}\Omega_s=(1-n)\mathrm{d}\Omega$ is the volume of the solid phase in the current configuration and $\mathrm{d}\Omega_{s0}=(1-n_0)\mathrm{d}\Omega_0$ is the volume of the solid phase in the reference configuration. As a result, the current porosity n is given by

$$n=1-(1-n_0)\frac{J_s}{J} \tag{7}$$

3. BALANCE EQUATIONS

The large strain balance equations for a porous medium saturated by a single fluid are well known ([8, 12, 54] for an overview, see also [55]) and are only briefly recalled here.

Let us denote with $\boldsymbol{v}_s(\boldsymbol{x},t)$ and $\boldsymbol{v}_w(\boldsymbol{x},t)$ the spatial description of the velocities of the solid and fluid phase respectively, and correspondingly, using Gurtin's notation [56], let $\dot{\boldsymbol{v}}_s(\boldsymbol{x},t)$ and $\dot{\boldsymbol{v}}_w(\boldsymbol{x},t)$

DOI: 10.1002/nme

be the spatial description of the accelerations. Equivalently, let $\dot{\boldsymbol{x}}(\boldsymbol{X},t)$ and $\ddot{\boldsymbol{x}}(\boldsymbol{X},t)$ be the material description of the velocity and acceleration of the solid phase, respectively.[§]

The spatial descriptions of the relative velocity and acceleration of the fluid phase with respect to the solid phase are denoted with $\boldsymbol{w}(\boldsymbol{x},t)$ and $\dot{\boldsymbol{w}}(\boldsymbol{x},t)$

$$\boldsymbol{w}(\boldsymbol{x},t)=\boldsymbol{v}_w(\boldsymbol{x},t)-\boldsymbol{v}_s(\boldsymbol{x},t) \quad \text{and} \quad \dot{\boldsymbol{w}}(\boldsymbol{x},t)=\dot{\boldsymbol{v}}_w(\boldsymbol{x},t)-\dot{\boldsymbol{v}}_s(\boldsymbol{x},t) \tag{8}$$

while their corresponding material descriptions are $\bar{\boldsymbol{w}}(\boldsymbol{X},t)=\boldsymbol{w}(\boldsymbol{\varphi}(\boldsymbol{X},t),t)$ and $\dot{\bar{\boldsymbol{w}}}(\boldsymbol{X},t)=\dot{\boldsymbol{w}}(\boldsymbol{\varphi}(\boldsymbol{X},t),t)$.

In the following the balance equations in the reference configuration $\mathscr{B}_0$ will be briefly recalled. For the sake of completeness the corresponding equations for the current configuration $\mathscr{B}$ are given in Appendix A.

3.1. Mass balance equation

In the current configuration $\mathscr{B}$, the mass flux $\boldsymbol{M}$ (*Cauchy* mass flux) is defined as

$$\boldsymbol{M}=n\rho_w\boldsymbol{w} \tag{9}$$

while in the reference configuration $\mathscr{B}_0$, the corresponding scaled quantity is the *Piola–Kirchhoff* mass flux

$$\boldsymbol{M}_R=J\boldsymbol{F}^{-1}\boldsymbol{M}, \tag{10}$$

thus

$$\boldsymbol{M}_R=n\rho_w J\boldsymbol{F}^{-1}\bar{\boldsymbol{w}} \tag{11}$$

For a porous material that is hydraulically isotropic in the reference configuration, according to Darcy's law we have

$$\boldsymbol{M}_R=-\rho_w\frac{K_D^0}{g}\mathrm{Grad}(\mu_w+U) \tag{12}$$

μ_w being the chemical potential of the pore fluid, which is defined as

$$\dot{\mu}_w=\frac{\dot{p}_w}{\rho_w} \tag{13}$$

where p_w is the positive pore fluid pressure (hence μ_w is a known function of p_w), K_D^0 is the hydraulic conductivity with the dimensions of a velocity, g is the gravity acceleration and U is the body force potential per unit mass (thus $\boldsymbol{b}_0=-\mathrm{Grad}U$, where $\boldsymbol{b}_0$ is the body force per unit mass in the reference configuration). Let us add that the chemical potential μ_w represents the free energy per unit mass of pore fluid.

The mass balance equation in the reference configuration $\mathscr{B}_0$ (as written by Biot [9], and later by [8]) is

$$\dot{\bar{m}}_w=-\mathrm{Div}\boldsymbol{M}_R \tag{14}$$

Although K_D^0 will be assumed to be constant in this work for the sake of simplicity, K_D^0 generally depends on the porosity through a relationship that can be described by one of the several empirical laws proposed in the literature (e.g. the Kozeny–Carman formula). In the case of initial anisotropic hydraulic conductivity (namely the hydraulic conductivity is anisotropic in the reference configuration), the scalar K_D^0 must be substituted by a second-order symmetric tensor (see [57] for a more detailed discussion on this point).

[§]Thus the following identities hold true: $\boldsymbol{v}_s(\boldsymbol{x},t)=\dot{\boldsymbol{x}}(\boldsymbol{\varphi}^{-1}(\boldsymbol{x},t),t)$ and $\dot{\boldsymbol{v}}_w(\boldsymbol{x},t)=\ddot{\boldsymbol{x}}(\boldsymbol{\varphi}^{-1}(\boldsymbol{x},t),t)$.

DOI: 10.1002/nme

3.2. Momentum balance equation for the whole porous medium

For an element volume moving with the solid phase, the momentum balance equation for the whole porous medium in the reference configuration $\mathscr{B}_0$ is

$$\overbrace{(1-n_0)\rho_{s0}\ddot{\boldsymbol{x}}+[n\rho_w J(\dot{\boldsymbol{x}}+\bar{\boldsymbol{w}})]^{\cdot}}^{(1)}=\overbrace{-\mathrm{Div}\,((\dot{\boldsymbol{x}}+\bar{\boldsymbol{w}})\otimes\boldsymbol{M}_R)}^{(2)}+\overbrace{\mathrm{Div}\,\boldsymbol{S}}^{(3)}+\overbrace{[(1-n_0)\rho_{s0}+n\rho_w J]\boldsymbol{b}_0}^{(4)} \tag{15}$$

where $\boldsymbol{b}_0$ is the body force per unit mass in the reference configuration and $\boldsymbol{S}$ is the *total* first Piola–Kirchhoff stress tensor ($\boldsymbol{S}=J\boldsymbol{T}\boldsymbol{F}^{-\mathrm{T}}$ with $\boldsymbol{T}$ the *total* Cauchy stress tensor). Note that Equation (15) coincides with the corresponding expression given by Coussy [12].

The physical meanings of the various terms of Equation (15) are as follows:

(1) rate of increase in momentum per unit of undeformed volume;
(2) rate of momentum gain by convection per unit of undeformed volume;
(3) traction forces on the infinitesimal porous volume per unit of undeformed volume; and
(4) gravitational forces on the infinitesimal porous volume per unit of undeformed volume.

From Equations (14) and (11), the rate of increase in momentum per unit of initial volume in the reference configurations can be expressed as follows:

$$[n\rho_w J(\dot{\boldsymbol{x}}+\bar{\boldsymbol{w}})]^{\cdot}=n\rho_w J(\ddot{\boldsymbol{x}}+\dot{\bar{\boldsymbol{w}}})-(\mathrm{Div}\,\boldsymbol{M}_R)(\dot{\boldsymbol{x}}+\bar{\boldsymbol{w}}) \tag{16}$$

Moreover, since

$$\mathrm{Div}\,[(\dot{\boldsymbol{x}}+\bar{\boldsymbol{w}})\otimes\boldsymbol{M}_R]=(\mathrm{Div}\,\boldsymbol{M}_R)(\dot{\boldsymbol{x}}+\bar{\boldsymbol{w}})+\mathrm{Grad}(\dot{\boldsymbol{x}}+\bar{\boldsymbol{w}})\boldsymbol{M}_R \tag{17}$$

the momentum balance equation in the reference configuration $\mathscr{B}_0$ becomes

$$\begin{aligned}(1-n_0)\rho_{s0}\ddot{\boldsymbol{x}}+n\rho_w J(\ddot{\boldsymbol{x}}+\dot{\bar{\boldsymbol{w}}})=&-n\rho_w J(\dot{\boldsymbol{F}}+\mathrm{Grad}\dot{\bar{\boldsymbol{w}}})\boldsymbol{F}^{-1}\bar{\boldsymbol{w}}\\&+\mathrm{Div}\,\boldsymbol{S}+[(1-n_0)\rho_{s0}+n\rho_w J]\boldsymbol{b}_0\end{aligned} \tag{18}$$

It is worth emphasizing that the term $n\rho_w J(\dot{\boldsymbol{F}}+\mathrm{Grad}\dot{\bar{\boldsymbol{w}}})\boldsymbol{F}^{-1}\bar{\boldsymbol{w}}$ in Equation (18) represents the convective fluid acceleration force.

3.3. Momentum balance equation for the pore fluid

Let $\boldsymbol{f}_{w0}$ and $\boldsymbol{f}_{s0}$ denote the body force accounting for the local interaction between the solid and fluid constituents in the reference configuration. In the literature, this effect is termed the *momentum supply* [58], hence $\boldsymbol{f}_{w0}$ is the momentum supplied by the solid phase to the fluid one, and obviously $\boldsymbol{f}_{s0}=-\boldsymbol{f}_{w0}$.

For an element volume moving with the solid phase, given Equation (18), the momentum balance equation for the pore fluid in the reference configuration $\mathscr{B}_0$ is

$$\begin{aligned}n\rho_w J(\ddot{\boldsymbol{x}}+\dot{\bar{\boldsymbol{w}}})=&-n\rho_w J(\dot{\boldsymbol{F}}+\mathrm{Grad}\dot{\bar{\boldsymbol{w}}})\boldsymbol{F}^{-1}\bar{\boldsymbol{w}}+n\mathrm{Div}\,(-Jp_w\boldsymbol{F}^{-\mathrm{T}})\\&+\boldsymbol{f}_{w0}+n\rho_w J\boldsymbol{b}_0\end{aligned} \tag{19}$$

where the momentum supply $\boldsymbol{f}_{w0}$ (per unit of volume in $\mathscr{B}_0$) is a constitutive assumption. A classical porous medium is considered in this work, hence the momentum supply is assumed to equate to

$$\boldsymbol{f}_{w0}=-nJ^2\frac{g}{K_D^0}\left(\frac{1}{J}\boldsymbol{F}^{-\mathrm{T}}\boldsymbol{M}_R\right)-J\rho_a\dot{\bar{\boldsymbol{w}}} \tag{20}$$

where ρ_a is the *virtual mass* per unit of deformed volume of saturated porous medium. In the literature, the added mass is usually expressed as

$$\rho_a=(\tau-1)n\rho_w \tag{21}$$

DOI: 10.1002/nme

where τ is the tortuosity that can be estimated from the porosity, n, using empirical relationships (e.g. [59]), or theoretical analyses [60]. The same considerations as for K_D^0 are applicable to the tortuosity τ as well, namely that τ must generally be represented by a second-order tensor in the case of an anisotropic pore structure in the reference configuration. The result is that the momentum supply depends on a *viscous drag* (represented by the first term of Equation (20)) and on an inertial coupling (given by the second term of Equation (20)), the effects of which have been analysed by Gajo [53, 61].¶

As observed by Bowen [7], the momentum supply, $\boldsymbol{f}_{w0}$, defined by Equation (20) does not respect the axiom of material frame-indifference because $\boldsymbol{f}_{w0}$ depends on inertial effects, hence its behaviour under a change of frame is similar to that of the other inertial forces constituting Newton's second law, which is not frame-invariant unless 'fictitious inertia forces' (such as centrifugal and Coriolis forces) are supplied when the frame of reference is rotating relative to an inertial frame [62].

Using the identity $\mathrm{Div}(-Jp_w\boldsymbol{F}^{-\mathrm{T}}) = -J\boldsymbol{F}^{-\mathrm{T}}\mathrm{Grad}(p_w)$, Equation (19) can thus be rewritten as

$$n\rho_w J(\ddot{\boldsymbol{x}}+\tau\ddot{\bar{\boldsymbol{w}}}) = -n\rho_w J(\dot{\boldsymbol{F}}+\mathrm{Grad}\dot{\bar{\boldsymbol{w}}})\boldsymbol{F}^{-1}\bar{\boldsymbol{w}} - n\rho_w J\boldsymbol{F}^{-\mathrm{T}}\mathrm{Grad}\mu_w$$
$$-n\frac{g}{K_D^0}J\boldsymbol{F}^{-\mathrm{T}}\boldsymbol{M}_R + n\rho_w J\boldsymbol{b}_0 \tag{22}$$

As a result, Equation (22) is reduced to Equation (12) in the case of permanent pore fluid flow ($\dot{\bar{\boldsymbol{w}}}=\boldsymbol{0}$), uniform motion of the solid skeleton (thus $\ddot{\boldsymbol{x}}=\boldsymbol{0}$) and negligible convective terms.

4. HYPERELASTIC CONSTITUTIVE EQUATIONS

Gajo [38] has recently formulated a general method for defining the free energy density function of an isotropic saturated porous media with compressible solid and fluid constituents, subjected to large deformations. The free energy thus defined is a potential for the stress-like quantities (namely the *total* first Piola–Kirchhoff stress tensor $\boldsymbol{S}$ and the chemical potential of pore water μ_w) with respect to the work-conjugate strain-like quantities (namely the deformation gradient $\boldsymbol{F}$ and the variation of fluid mass content $\bar{m}_w$), namely

$$\boldsymbol{S} = \frac{\partial\psi_0(\boldsymbol{F},\bar{m}_w)}{\partial\boldsymbol{F}} \quad \text{and} \quad \mu_w = \frac{\partial\psi_0(\boldsymbol{F},\bar{m}_w)}{\partial\bar{m}_w} \tag{23}$$

The main limitation of the proposed approach lies in the admissible behvaiour of the solid constituent, which must have a linear response in the logarithmic volume strain (see Equations (26) and (28), later on).

According to Gajo [38], assuming also for the solid skeleton and the pore fluid a linear behaviour in the logarithmic volume strain, the proposed hyperelastic formulation leads to the

$$\boldsymbol{S} = \overbrace{\underbrace{\mathscr{K}(\mathrm{Ln}J-\mathrm{Ln}J_{s-f})\boldsymbol{F}^{-\mathrm{T}}}_{\boldsymbol{S}'_{\mathrm{vol}}} - Jp_w\boldsymbol{F}^{-\mathrm{T}}}^{\boldsymbol{S}_{\mathrm{vol}}} + \overbrace{\mu J^{-2/3}[\boldsymbol{F}-\frac{1}{3}(\boldsymbol{F}\bullet\boldsymbol{F})\boldsymbol{F}^{-\mathrm{T}}]}^{\boldsymbol{S}_{\mathrm{iso}}=\boldsymbol{S}'_{\mathrm{iso}}} \tag{24}$$

$$\mu_w = -\mathscr{K}_w\frac{nJ}{m_w} + \frac{\mathscr{K}_w}{\rho_{w0}} \tag{25}$$

¶In Equation (20) the expression of the inertial coupling has been obtained by simply extending to large strains the equivalent expression for small strains. It is worth recalling that, by averaging microscopic quantities, Coussy [12] obtained a slightly different value, which would imply that

$\boldsymbol{f}_{w0} = -nJ\frac{g}{K_D^0}(\boldsymbol{F}^{-\mathrm{T}}\boldsymbol{M}_R) - J\rho_a\dot{\bar{\boldsymbol{w}}} + J\rho_a\bar{\boldsymbol{w}}\boldsymbol{D}$ where $\boldsymbol{D}$ is the rate of deformation tensor.

DOI: 10.1002/nme

where $\boldsymbol{S}'_{\text{vol}}$ and $\boldsymbol{S}'_{\text{iso}}$ are the *volumetric* and *isochoric* (i.e. volume preserving) contributions of the *effective* first Piola–Kirchhoff stress tensor, $\boldsymbol{S}'=\boldsymbol{S}'_{\text{vol}}+\boldsymbol{S}'_{\text{iso}}=\boldsymbol{S}+Jp_w\boldsymbol{F}^{-\text{T}}$ is the *effective* first Piola–Kirchhoff stress tensor, p_w is the pore pressure, μ and $\mathscr{K}$ are constitutive parameters acting as the shear and bulk stiffness of the solid skeleton, respectively, and $\mathscr{K}_w$ is a constitutive parameter acting as the bulk stiffness of the fluid constituent. Finally J_{s-f} is the volume compression of the solid constituent due to the pore fluid

$$\text{Ln}J_{s-f}=-(J_s p_w)/\mathscr{K}_s \tag{26}$$

where $\mathscr{K}_s$ is a constitutive parameter acting as the bulk stiffness of the solid constituent and J_s is the *total* volume compression of the solid constituents

$$J_s=J_{s-m}J_{s-f} \tag{27}$$

where J_{s-m} is the volume compression of the solid constituent due to intergranular contact stresses

$$\text{Ln}J_{s-m}=\text{tr}(\boldsymbol{S}'\boldsymbol{F}^{\text{T}})/[3(1-n_0)\mathscr{K}_s] \tag{28}$$

with $\boldsymbol{K}'=\boldsymbol{S}'\boldsymbol{F}^{\text{T}}=\boldsymbol{K}+Jp_w\boldsymbol{I}$ the *effective* Kirchhoff stress tensor.

It is worth noting that substituting Equation (26) into Equation (24), we recover that

$$\boldsymbol{S}=\boldsymbol{S}''-\alpha Jp_w\boldsymbol{F}^{-\text{T}} \tag{29}$$

with

$$\alpha=1-\frac{J_s\mathscr{K}}{J\mathscr{K}_s}$$

$$\boldsymbol{S}''=\mathscr{K}\text{Ln}J\boldsymbol{F}^{-\text{T}}+\mu J^{-2/3}\left[\boldsymbol{F}-\tfrac{1}{3}(\boldsymbol{F}\bullet\boldsymbol{F})\boldsymbol{F}^{-\text{T}}\right]$$

Thus Equation (29) represents the extension to large strains of the effective stress proposed by Nur and Byerlee [49] for small strains. This extension was obtained by Gajo [38] by assuming a well-defined constitutive response of the solid constituent (i.e. the volume component of the Kirchhoff stress admits a linear behaviour in the logarithmic volumetric strain) and by rigorously treating the effects of solid constituent compression due to the fluid pressure under large strain, in the same way as for a thermal strain. This approach leads to a different definition of the effective stress from those given by other Authors for large strain analysis of porous media with compressible solid constituents, namely Borja [48]—who recovered the small strain definition given by Nur and Byerlee [49] by reasoning in terms of Cauchy stress tensor in the current configuration—and Bluhm and de Boer [43]—who restricted their general, large-strain framework to the definition of effective stress proposed by Suklje [45] for small strains.

When $\boldsymbol{S}$ and μ_w (and consequently p_w) are known, J_{s-f} can be obtained from Equation (26), by taking Equations (27) and (24) into account. The resulting non-linear equation can be solved with the Newton–Raphson algorithm, in which the residuum δR is given by Equation (26), namely $\delta R=p_w+\mathscr{K}_s\text{Ln}J_{s-f}/J_s$, while the correction δJ_{s-f} is obtained from

$$\delta J_{s-f}=-J_{s-f}\left(\frac{1}{J_s}+\frac{p_w}{\mathscr{K}_s}-\frac{\mathscr{K}p_w}{\mathscr{K}_s^2(1-n_0)}\right)^{-1}\frac{\delta R}{\mathscr{K}_s} \tag{30}$$

Finally the rate equations in terms of $\boldsymbol{S}$ and $\boldsymbol{F}$ become

$$\begin{bmatrix}\dot{\boldsymbol{S}}\\ \dot{\mu}_w\end{bmatrix}=\begin{bmatrix}\mathbb{H} & c\boldsymbol{F}^{-\text{T}}\\ c\boldsymbol{F}^{-\text{T}} & d\end{bmatrix}\begin{bmatrix}\dot{\boldsymbol{F}}\\ \dot{\bar{m}}_w\end{bmatrix} \tag{31}$$

DOI: 10.1002/nme

with

$$c=-\beta\frac{\mathscr{K}_w}{m_w}\frac{\alpha+r(1-a)}{1+r(1-a)}J,\quad d=\beta\frac{\mathscr{K}_w}{m_w}\frac{nJ}{m_w} \tag{32}$$

$$\beta=\left(1+\frac{\mathscr{K}_w}{m_w}\frac{J_s^2(1-n_0)(1-a)}{\mathscr{K}_s(1+r(1-a))}\rho_w\right)^{-1} \tag{33}$$

$$a=\frac{\mathscr{K}}{\mathscr{K}_s(1-n_0)},\quad r=\frac{J_s p_w}{\mathscr{K}_s} \tag{34}$$

and finally

$$\begin{aligned}\mathbb{H}=&\left[\mathscr{K}+\frac{\mathscr{K}^2}{\mathscr{K}_s(1-n_0)}\frac{r}{1+r(1-a)}-Jp_w+\beta\mathscr{K}_w\left(\frac{\alpha+r(1-a)}{1+r(1-a)}\right)^2\frac{J}{n}\right]\boldsymbol{F}^{-\mathrm{T}}\otimes\boldsymbol{F}^{-\mathrm{T}}\\&-\left[\mathscr{K}(\mathrm{Ln}J-\mathrm{Ln}J_{s-f})-Jp_w\right]\boldsymbol{F}^{-\mathrm{T}}\underline{\otimes}\boldsymbol{F}^{-1}\\&+\mu J^{-2/3}\left(\boldsymbol{I}\overline{\otimes}\boldsymbol{I}+\frac{(\boldsymbol{F}\bullet\boldsymbol{F})}{3}\boldsymbol{F}^{-\mathrm{T}}\underline{\otimes}\boldsymbol{F}^{-1}+\frac{2(\boldsymbol{F}\bullet\boldsymbol{F})}{9}\boldsymbol{F}^{-\mathrm{T}}\otimes\boldsymbol{F}^{-\mathrm{T}}\right)\\&-\frac{2}{3}\mu J^{-2/3}(\boldsymbol{F}^{-\mathrm{T}}\otimes\boldsymbol{F}+\boldsymbol{F}\otimes\boldsymbol{F}^{-\mathrm{T}})\end{aligned} \tag{35}$$

It is worth noting that, for certain combinations of the constitutive parameters, it may be that β^{-1} is null or even negative, leading to a tangent operator (in Equation (31)) that is not positive definite.[‖] This typically happens when the ratio $\mathscr{K}/\mathscr{K}_s\approx 1$ and n_0 is large (hence the term $1-a$ may become negative, although this would be rather unrealistic), combined with high values of $\mathscr{K}_w$.

5. FINITE ELEMENT FORMULATIONS

The field equations to satisfy are the mass balance equation (Equations (14) and (A2), for the reference and the current configurations, respectively), and the momentum balance equations for the whole saturated porous medium (Equations (18) and (A6)) and for the pore fluid (Equations (22) and (A7)).

The material setting has been preferred here, hence the field equations are written in the reference configuration. An entirely similar formulation could have been obtained in the current configuration, however.

5.1. Complete version of the finite element formulation

If we consider the complete version of the balance equations, the selected primary unknown fields are: the non-linear map $\boldsymbol{\varphi}$, the relative pore fluid velocities with respect to the solid velocities $\bar{\boldsymbol{w}}$, the *Piola–Kirchhoff* mass flux $\boldsymbol{M}_R$ and the chemical potential of the pore fluid μ_w (which is a known function of the pore pressure p_w). The reference placements $\boldsymbol{X}$ and the unknown fields are interpolated, within the generic element e, in terms of nodal values and shape functions $\boldsymbol{N}_u$, $\boldsymbol{N}_w$ and $\boldsymbol{N}_\mu$, so that

$$\boldsymbol{X}=\boldsymbol{N}_u\boldsymbol{X}^e,\quad \boldsymbol{x}=\boldsymbol{\varphi}=\boldsymbol{N}_u\boldsymbol{\Psi}^e,\quad \bar{\boldsymbol{w}}=\boldsymbol{N}_w\boldsymbol{W}^e,\quad \boldsymbol{M}_R=\boldsymbol{N}_w\boldsymbol{\Omega}^e,\ \mu_w=\boldsymbol{N}_\mu\boldsymbol{\Pi}_w^e \tag{36}$$

In analogy to the three-field finite element formulation for the dynamic behaviour under small strains [22], biquadratic Lagrangian shape functions have been selected for $\boldsymbol{N}_u$ and $\boldsymbol{N}_w$ and bilinear

[‖]The condition $\beta^{-1}=0$ is equivalent to $\tilde{Q}=0$ in the small strain formulation (see Section 6.2 for the meaning of the symbols).

DOI: 10.1002/nme

shape functions for $\boldsymbol{N}_\mu$. It is worth recalling that Markert *et al.* [36] recently performed accuracy analyses of quadratic-linear interpolation functions (for the solid displacements on the one hand, and for the fluid velocity and the pore pressure on the other), comparing them with equal-order interpolation functions (i.e. linear–linear and quadratic–quadratic) for a three-field formulation for the dynamic behaviour of saturated porous media with incompressible solid and fluid constituents. The analysis conducted by Markert *et al.* [36] is not applicable to our case, however, because they considered an equal interpolation order for the absolute fluid velocity and the pore pressure.

The weak form of the problem is obtained by performing a scalar multiplication of the three field equations by the virtual fields $\delta\boldsymbol{\varphi}$, $\delta\bar{\boldsymbol{w}}$ and $\delta\mu_w$ and integrating by parts over the reference configuration $\mathscr{B}_0$, thus obtaining for the momentum balance equation of the whole porous medium

$$\begin{aligned}&\int_{\mathscr{B}_0}[(1-n_0)\rho_{s0}+n\rho_w J](\delta\boldsymbol{\varphi})\bullet\ddot{\boldsymbol{x}}\,\mathrm{d}V_0+\int_{\mathscr{B}_0}(n\rho_w J)(\delta\boldsymbol{\varphi})\bullet\dot{\bar{\boldsymbol{w}}}\,\mathrm{d}V_0\\&\quad+\int_{\mathscr{B}_0}(\dot{\boldsymbol{F}}+\nabla\dot{\bar{\boldsymbol{w}}})\bullet(\delta\bar{\boldsymbol{w}}\otimes\boldsymbol{M}_R)\mathrm{d}V_0+\int_{\mathscr{B}_0}\nabla(\delta\boldsymbol{\varphi})\bullet\boldsymbol{S}\,\mathrm{d}V_0\\&=\int_{\mathscr{B}_0}[(1-n_0)\rho_{s0}+n\rho_w J](\delta\boldsymbol{\varphi})\bullet\boldsymbol{b}_0\mathrm{d}V_0+\int_{\partial\mathscr{B}_0}(\delta\boldsymbol{\varphi})\bullet(\boldsymbol{S}\boldsymbol{n}_0)\mathrm{d}A_0\end{aligned}\tag{37}$$

where $\boldsymbol{n}_0$ is the unit outward normal to the boundary $\partial\mathscr{B}_0$ and $(\boldsymbol{S}\boldsymbol{n}_0)$ are the surface tractions acting in the reference configuration, ∇ is the gradient operator in the reference configuration ($\nabla=\mathrm{Grad}$), hence $\boldsymbol{F}=(\nabla\boldsymbol{N}_u)\boldsymbol{\varphi}$ and $\dot{\boldsymbol{F}}=(\nabla\boldsymbol{N}_u)\dot{\boldsymbol{\varphi}}$. The symbol '$\bullet$' denotes the scalar product.

After integration by parts, the weak form of the momentum balance of the pore fluid becomes

$$\begin{aligned}&\int_{\mathscr{B}_0}(n\rho_w J)(\delta\bar{\boldsymbol{w}})\bullet\ddot{\boldsymbol{x}}\,\mathrm{d}V_0+\int_{\mathscr{B}_0}[\tau n\rho_w J](\delta\bar{\boldsymbol{w}})\bullet\dot{\bar{\boldsymbol{w}}}\,\mathrm{d}V_0\\&\quad+\int_{\mathscr{B}_0}(\dot{\boldsymbol{F}}+\nabla\dot{\bar{\boldsymbol{w}}})\bullet(\delta\bar{\boldsymbol{w}}\otimes\boldsymbol{M}_R)\mathrm{d}V_0+\int_{\mathscr{B}_0}(n\rho_w J)(\delta\bar{\boldsymbol{w}})\bullet(\boldsymbol{F}^{-\mathrm{T}}\nabla\mu_w)\mathrm{d}V_0\\&\quad+\int_{\mathscr{B}_0}\left(n\frac{g}{K_D^0}J(n\rho_w J)\right)(\delta\bar{\boldsymbol{w}})\bullet(\boldsymbol{B}^{-1}\bar{\boldsymbol{w}})\mathrm{d}V_0=\int_{\mathscr{B}_0}(n\rho_w J)(\delta\bar{\boldsymbol{w}})\bullet\boldsymbol{b}_0\mathrm{d}V_0\end{aligned}\tag{38}$$

where $\boldsymbol{B}=\boldsymbol{F}\boldsymbol{F}^{\mathrm{T}}$ is the left Cauchy–Green deformation tensor. Finally the weak form of the mass balance of the pore fluid can be obtained by considering the rate constitutive relationships, namely Equation (31) for the elastic response, thus $\dot{\bar{m}}_w$ equates to

$$\dot{\bar{m}}_w=\frac{1}{d}\dot{\mu}_w-\frac{c}{d}(\boldsymbol{F}^{-\mathrm{T}}\bullet\dot{\boldsymbol{F}})\tag{39}$$

As a result, from Equations (14), the weak form of the mass balance of the pore fluid is reduced to

$$\int_{\mathscr{B}_0}(\delta\mu_w)\mathrm{Div}\boldsymbol{M}_R\mathrm{d}V_0-\int_{\mathscr{B}_0}(\delta\mu_w)\frac{c}{d}(\boldsymbol{F}^{-\mathrm{T}}\bullet\dot{\boldsymbol{F}})\mathrm{d}V_0+\int_{\mathscr{B}_0}(\delta\mu_w)\frac{1}{d}\dot{\mu}_w\mathrm{d}V_0=0\tag{40}$$

Finally, the weak form of Equation (11) leads to

$$\int_{\mathscr{B}_0}(\delta\bar{\boldsymbol{w}})\bullet\boldsymbol{M}_R\mathrm{d}V_0=\int_{\mathscr{B}_0}(n\rho_w J)(\delta\bar{\boldsymbol{w}})\bullet\boldsymbol{F}^{-1}\bar{\boldsymbol{w}}\mathrm{d}V_0\tag{41}$$

Note that Equation (41) can be solved at element level

$$\boldsymbol{\Omega}^e=(\boldsymbol{D}_e^{-1}\boldsymbol{A}_e)\boldsymbol{W}^e\tag{42}$$

DOI: 10.1002/nme

where

$$\boldsymbol{D}_e = \int_{V^e} \boldsymbol{N}_w^{\mathrm{T}} \boldsymbol{N}_w \mathrm{d}V^e \quad \text{and} \quad \boldsymbol{A}_e = \int_{V^e} \boldsymbol{N}_w^{\mathrm{T}} [n\rho_w J \boldsymbol{F}^{-1}] \boldsymbol{N}_w \mathrm{d}V^e \tag{43}$$

The primary unknown fields are thus reduced to just three, i.e. $\boldsymbol{\varphi}$, $\bar{\boldsymbol{w}}$ and μ_w.

It is worth adding that from Equation (13), the mass and momentum balance equations could be written in terms of the pore pressure p_w, instead of the chemical potential μ_w. The latter was preferred as one of the primary unknowns, however, because this choice improves the conditioning of the system for solving the algebric equations and it has theoretical implications in non-isothermal problems (e.g. [12]).

Let $\mathscr{X}$ denote the unknown vector

$$\mathscr{X} = [\boldsymbol{\Psi} \quad \boldsymbol{\Pi} \quad \boldsymbol{W}]^{\mathrm{T}}, \quad \dot{\mathscr{X}} = [\dot{\boldsymbol{\Psi}} \quad \dot{\boldsymbol{\Pi}} \quad \dot{\boldsymbol{W}}]^{\mathrm{T}}, \quad \ddot{\mathscr{X}} = [\ddot{\boldsymbol{\Psi}} \quad \boldsymbol{0} \quad \boldsymbol{0}]^{\mathrm{T}} \tag{44}$$

and $\mathscr{R}$ the residual vector

$$\mathscr{R} = \mathscr{R}^{\mathrm{dyn}}(\mathscr{X}, \ddot{\mathscr{X}}) + \mathscr{R}^{\mathrm{vis}}(\mathscr{X}, \dot{\mathscr{X}}) + \mathscr{R}^{\mathrm{int}}(\mathscr{X}) - \mathscr{R}^{\mathrm{ext}}(\mathscr{S}, \mathscr{X}) = \mathscr{O} \tag{45}$$

where $\mathscr{R}^{\mathrm{dyn}}$ is the vector containing inertial effects and $\mathscr{R}^{\mathrm{vis}}$ contains the viscous internal forces. In general, they should include the convective acceleration forces, which have to be treated numerically with a special stabilization method. In most applications the convective acceleration forces are negligible, hence we neglect them below. Furthermore, $\mathscr{R}^{\mathrm{int}}$ contains the elastic internal forces, and $\mathscr{R}^{\mathrm{ext}}$ contains the surface loadings (denoted collectively by $\mathscr{S}$) and the external body forces

$$\mathscr{R}^{\mathrm{ext}} = \begin{bmatrix} \displaystyle\int_{\partial V^e} \boldsymbol{N}_u^{\mathrm{T}} (\boldsymbol{S}\boldsymbol{n}_0) \mathrm{d}A^e + \int_{V^e} \boldsymbol{N}_u^{\mathrm{T}} [(1-n_0)\rho_{s0} + n\rho_w J] \boldsymbol{b}_0 \mathrm{d}V^e \\ \boldsymbol{0} \\ \displaystyle\int_{V^e} \boldsymbol{N}_w^{\mathrm{T}} (n\rho_w J) \boldsymbol{b}_0 \mathrm{d}V^e \end{bmatrix} \tag{46}$$

$$\mathscr{R}^{\mathrm{int}} = \begin{bmatrix} \displaystyle\int_{V^e} (\nabla \boldsymbol{N}_u)^{\mathrm{T}} \boldsymbol{S} \mathrm{d}V^e \\ \boldsymbol{0} \\ \displaystyle\int_{V^e} \boldsymbol{N}_w^{\mathrm{T}} (n\rho_w J) \boldsymbol{F}^{-\mathrm{T}} \nabla \mu_w \mathrm{d}V^e \end{bmatrix} \tag{47}$$

$$\mathscr{R}^{\mathrm{dyn}} = \begin{bmatrix} \displaystyle\int_{V^e} \boldsymbol{N}_u^{\mathrm{T}} [(1-n_0)\rho_{s0} + n\rho_w J] \ddot{\boldsymbol{x}} \mathrm{d}V^e + \int_{V^e} \boldsymbol{N}_u^{\mathrm{T}} (n\rho_w J) \dot{\bar{\boldsymbol{w}}} \mathrm{d}V^e \\ \boldsymbol{0} \\ \displaystyle\int_{V^e} \boldsymbol{N}_w^{\mathrm{T}} (n\rho_w J) \ddot{\boldsymbol{x}} \mathrm{d}V^e + \int_{V^e} \boldsymbol{N}_w^{\mathrm{T}} (\tau n\rho_w J) \dot{\bar{\boldsymbol{w}}} \mathrm{d}V^e \end{bmatrix} \tag{48}$$

$$\mathscr{R}^{\mathrm{vis}} = \begin{bmatrix} \boldsymbol{0} \\ \displaystyle\int_{V^e} \boldsymbol{N}_\mu^{\mathrm{T}} (-(\boldsymbol{I} \bullet \nabla \boldsymbol{M}_R) + (1/d)\dot{\mu}_w - (c/d)(\boldsymbol{F}^{-\mathrm{T}} \bullet \dot{\boldsymbol{F}})) \mathrm{d}V^e \\ \displaystyle\int_{V^e} \boldsymbol{N}_w^{\mathrm{T}} \left(ngJ(n\rho_w J)/K_D^0 \right) \boldsymbol{B}^{-1} \bar{\boldsymbol{w}} \mathrm{d}V^e \end{bmatrix} \tag{49}$$

In Section 5.3, we propose the discontinuous Galerkin FEM in the time domain for the accurate time integration of the governing equations in the case of wave propagation.

DOI: 10.1002/nme

For the purposes of comparison, however, we introduce here the well-known Newmark scheme for the time integration of the semi-discrete equations. In this case, the unknown vector quantities at time $t+\Delta t$ are assumed to be expressed as

$$\mathscr{X}^{(k)}_{t+\Delta t} = \mathscr{X}^{(k-1)}_{t+\Delta t} + \Delta\mathscr{X}^{(k)} \tag{50}$$

$$\dot{\mathscr{X}}^{(k)}_{t+\Delta t} = \left(1-\frac{\delta}{\alpha}\right)\dot{\mathscr{X}}_t + \left(1-\frac{\delta}{2\alpha}\right)\ddot{\mathscr{X}}_t\Delta t + \frac{\delta}{\alpha\Delta t}\left(\mathscr{X}^{(k-1)}_{t+\Delta t} - \mathscr{X}_t + \Delta\mathscr{X}^{(k)}\right) \tag{51}$$

$$\ddot{\mathscr{X}}^{(k)}_{t+\Delta t} = \left(1-\frac{1}{2\alpha}\right)\ddot{\mathscr{X}}_t - \frac{1}{\alpha\Delta t}\dot{\mathscr{X}}_t + \frac{1}{\alpha\Delta t^2}\left(\mathscr{X}^{(k-1)}_{t+\Delta t} - \mathscr{X}_t + \Delta\mathscr{X}^{(k)}\right) \tag{52}$$

where k denotes the kth iteration. The Newmark scheme coincides with the trapezoidal rule for $\alpha=0.25$ and $\delta=0.50$. Let $\mathscr{R}_{t+\Delta t}$ denote the residual vector at time $t+\Delta t$. Using the modified Newton-Raphson iteration scheme, the governing equations are

$$\mathscr{M}^{(k-1)}_{t+\Delta t}\ddot{\mathscr{X}}^{(k)}_{t+\Delta t} + \mathscr{C}^{(k-1)}_{t+\Delta t}\dot{\mathscr{X}}^{(k)}_{t+\Delta t} + \mathscr{K}^{(k-1)}_{t+\Delta t}\Delta\mathscr{X}^{(k)} = (\mathscr{R}^{\text{ext}}_{t+\Delta t})^{(k-1)} - (\mathscr{R}^{\text{int}}_{t+\Delta t})^{(k-1)} \tag{53}$$

where $\mathscr{M}=\partial\mathscr{R}^{\text{dyn}}/\partial\ddot{\mathscr{X}}$ and $\mathscr{C}=\partial\mathscr{R}^{\text{vis}}/\partial\dot{\mathscr{X}}$ are the mass and viscous block matrices, and $\mathscr{K}=\mathscr{K}_1+\mathscr{K}_2+\mathscr{K}_3$ is the stiffness block matrix, where $\mathscr{K}_1=\partial\mathscr{R}^{\text{int}}/\partial\mathscr{X}$, $\mathscr{K}_2=\partial(\mathscr{R}^{\text{dyn}}+\mathscr{R}^{\text{vis}})/\partial\mathscr{X}$ and $\mathscr{K}_3=\partial\mathscr{R}^{\text{ext}}/\partial\mathscr{X}$. The element contributions to the block structures $\mathscr{M}$, $\mathscr{C}$ and $\mathscr{K}$ are not given for the sake of brevity. Thus, substituting into Equation (53), we obtain

$$\hat{\mathscr{K}}^{(k-1)}_{t+\Delta t}\Delta\mathscr{X}^{(k)} = -\mathscr{R}^{(k-1)}_{t+\Delta t} \tag{54}$$

with

$$\hat{\mathscr{K}} = \mathscr{K} + \frac{1}{\alpha\Delta t^2}\mathscr{M} + \frac{\delta}{\alpha\Delta t}\mathscr{C} \tag{55}$$

5.2. *Simplified version of finite element formulation*

In the case of a negligible relative acceleration of the pore fluid with respect to the solid skeleton ($\dot{\boldsymbol{w}}\approx\mathbf{0}$) and negligible convective terms, the momentum balance equation of the whole porous medium can obviously be simplified to become in the reference configuration

$$[(1-n_0)\rho_{s0}+n\rho_w J]\ddot{\boldsymbol{x}} = \text{Div}\,\boldsymbol{S} + [(1-n_0)\rho_{s0}+n\rho_w J]\boldsymbol{b}_0 \tag{56}$$

From the momentum balance equation of the pore fluid in the reference configuration we obtain

$$n\rho_w J\ddot{\boldsymbol{x}} = -n\rho_w J\boldsymbol{F}^{-\text{T}}\text{Grad}\mu_w - nJ\frac{g}{K^0_D}\boldsymbol{F}^{-\text{T}}\boldsymbol{M}_R + n\rho_w J\boldsymbol{b}_0 \tag{57}$$

hence the pore fluid mass flux is

$$\boldsymbol{M}_R = \rho_w\frac{K^0_D}{g}\boldsymbol{F}^{\text{T}}(-\ddot{\boldsymbol{x}} - \boldsymbol{F}^{-\text{T}}\text{Grad}\mu_w + \boldsymbol{b}_0) \tag{58}$$

The mass flux thus obtained from Equation (58) is then substituted into the pore fluid mass balance equation (Equation (14)), obtaining the expression of the pore fluid mass balance equation that is used in the present formulation.

The weak form of the problem in the reference configuration is obtained by multiplying the momentum balance equation and the pore fluid mass balance equation by the virtual fields $\delta\boldsymbol{\varphi}$ and $\delta\mu_w$ and integrating by parts over $\mathscr{B}_0$, thus leading to the following expression for the momentum balance equation:

$$\begin{aligned}\int_{\mathscr{B}_0}[(1-n_0)\rho_{s0}+n\rho_w J](\delta\boldsymbol{\varphi})\cdot\ddot{\boldsymbol{x}}\,\text{d}V_0 + \int_{\mathscr{B}_0}\nabla(\delta\boldsymbol{\varphi})\cdot\boldsymbol{S}\,\text{d}V_0 \\ = \int_{\mathscr{B}_0}[(1-n_0)\rho_{s0}+n\rho_w J](\delta\boldsymbol{\varphi})\cdot\boldsymbol{b}_0\,\text{d}V_0 + \int_{\partial\mathscr{B}_0}(\delta\boldsymbol{\varphi})\cdot(\boldsymbol{S}\boldsymbol{n}_0)\,\text{d}A_0\end{aligned} \tag{59}$$

DOI: 10.1002/nme

and for the pore fluid mass balance equation

$$\int_{\mathscr{B}_0}(\delta\mu_w)\dot{\bar{m}}_w \mathrm{d}V_0+\int_{\mathscr{B}_0}\left(\rho_w\frac{K_D^0}{g}\right)\nabla(\delta\mu_w)\bullet\nabla\mu_w \mathrm{d}V_0$$
$$+\int_{\mathscr{B}_0}\left(\rho_w\frac{K_D^0}{g}\right)\nabla(\delta\mu_w)\bullet\left(\boldsymbol{F}^{\mathrm{T}}\ddot{\boldsymbol{x}}\right)\mathrm{d}V_0=\int_{\mathscr{B}_0}\left(\rho_w\frac{K_D^0}{g}\right)\nabla(\delta\mu_w)\bullet\left(\boldsymbol{F}^{\mathrm{T}}\boldsymbol{b}_0\right)\mathrm{d}V_0$$
$$-\int_{\partial\mathscr{B}_0}(\delta\mu_w)(\boldsymbol{M}_R\bullet\boldsymbol{n}_0)\mathrm{d}A_0 \tag{60}$$

where $(\boldsymbol{M}_R\bullet\boldsymbol{n}_0)$ is the mass flux outflow from the boundary surface $\partial\mathscr{B}_0$ and $\dot{\bar{m}}_w$ is given by the constitutive equation (Equation (39)). In the case of elastic response, the first term of the weak form (Equation (60)) is reduced to

$$\int_{\mathscr{B}_0}(\delta\mu_w)\dot{\bar{m}}_w \mathrm{d}V_0=\int_{\mathscr{B}_0}\frac{1}{d}(\delta\mu_w)\dot{\mu}_w \mathrm{d}V_0-\int_{\mathscr{B}_0}\frac{c}{d}(\delta\mu_w)(\boldsymbol{F}^{-\mathrm{T}}\bullet\dot{\boldsymbol{F}})\mathrm{d}V_0 \tag{61}$$

Let $\mathscr{X}$ denote the unknown vector

$$\mathscr{X}=[\boldsymbol{\Psi}\ \boldsymbol{\Pi}]^{\mathrm{T}} \tag{62}$$

and $\mathscr{R}$ the residual vector

$$\mathscr{R}=\mathscr{R}^{\mathrm{dyn}}(\mathscr{X},\ddot{\mathscr{X}})+\mathscr{R}^{\mathrm{vis}}(\mathscr{X},\dot{\mathscr{X}})+\mathscr{R}^{\mathrm{int}}(\mathscr{X})-\mathscr{R}^{\mathrm{ext}}(\mathscr{S},\mathscr{X})=\mathscr{O} \tag{63}$$

where $\mathscr{R}^{\mathrm{dyn}}$ is the vector containing inertial effects, $\mathscr{R}^{\mathrm{vis}}$ contains the viscous internal forces, $\mathscr{R}^{\mathrm{int}}$ contains the elasto-plastic and viscous internal forces and $\mathscr{R}^{\mathrm{ext}}$ contains the surface loads (denoted collectively with $\mathscr{S}$) and the external body forces

$$\mathscr{R}^{\mathrm{ext}}=\begin{bmatrix}\displaystyle\int_{\partial V^e}\boldsymbol{N}_u^{\mathrm{T}}\boldsymbol{S}\boldsymbol{n}_0\mathrm{d}A^e+\int_{V^e}\boldsymbol{N}_u^{\mathrm{T}}[(1-n_0)\rho_{s0}+n\rho_w J]\boldsymbol{b}_0\mathrm{d}V^e\\ \displaystyle-\int_{\partial V^e}\boldsymbol{N}_\mu^{\mathrm{T}}(\boldsymbol{M}_R\bullet\boldsymbol{n}_0)\mathrm{d}A^e+\int_{V^e}(\nabla\boldsymbol{N}_\mu)^{\mathrm{T}}(\rho_w K_D^0/g)(\boldsymbol{F}^{\mathrm{T}}\boldsymbol{b}_0)\mathrm{d}V^e\end{bmatrix} \tag{64}$$

$$\mathscr{R}^{\mathrm{int}}=\begin{bmatrix}\displaystyle\int_{V^e}(\nabla\boldsymbol{N}_u)\boldsymbol{S}\mathrm{d}V^e\\ \displaystyle\int_{V^e}(\nabla\boldsymbol{N}_\mu)^{\mathrm{T}}(\rho_w K_D^0/g)(\nabla\mu_w)\mathrm{d}V_0\end{bmatrix} \tag{65}$$

$$\mathscr{R}^{\mathrm{dyn}}=\begin{bmatrix}\displaystyle\int_{V^e}\boldsymbol{N}_u[(1-n_0)\rho_{s0}+n\rho_w J]\ddot{\boldsymbol{x}}\mathrm{d}V^e\\ \displaystyle\int_{V^e}(\nabla\boldsymbol{N}_\mu)^{\mathrm{T}}(\rho_w K_D^0/g)(\boldsymbol{F}^{\mathrm{T}}\ddot{\boldsymbol{x}})\mathrm{d}V^e\end{bmatrix} \tag{66}$$

$$\mathscr{R}^{\mathrm{vis}}=\begin{bmatrix}\boldsymbol{0}\\ \displaystyle\int_{V^e}\boldsymbol{N}_\mu^{\mathrm{T}}(-(c/d)\boldsymbol{F}^{-\mathrm{T}}\bullet\dot{\boldsymbol{F}}+(1/d)\dot{\mu}_w)\mathrm{d}V^e\end{bmatrix} \tag{67}$$

According to Li *et al.* [63], biquadratic Lagrangian shape functions have been selected for $\boldsymbol{N}_u$ and bilinear shape functions for $\boldsymbol{N}_\mu$ in order to fulfill the Babuska–Brezzi condition (or the Zienckiewicz–Taylor patch test [64]). Time integration has been performed by using only Newmark method, according to the procedure described in Section 5.1, in fact the present simplified version is not reliable for studying wave propagation.

DOI: 10.1002/nme

5.3. The discontinuous Galerkin FEM for wave propagation problems

It is generally accepted that the Newmark method (like other equivalent time integration methods based on the finite difference method in the time domain) is best suited to dynamic problems dominated by a low frequency response [41]. The discontinuous Galerkin FEM in the time domain was implemented to improve the numerical response of the three-field formulation to the propagation of impulsive waves (involving discontinuities and sharp gradients).

The version of this method implemented here was inspired by Li *et al.* [41] and Chen *et al.* [65] for single-phase media, who reduced the computational cost by assuming continuous displacements and discontinuous velocities in time. For an alternative approach for saturated porous media in the case of incompressible constituents, see Chen *et al.* [35]. The implementation of the discontinuous Galerkin method will be discussed only for the complete, three-field finite element procedure, because both the discontinuous Galerkin method and the three-field finite element procedure are suited for studying the propagation of high frequency input pulses in saturated porous media.

Let us denote with $\lambda_1(t)$ and $\lambda_2(t)$ the (linear) shape functions in the time step $\Delta t = t_{n+1} - t_n$, hence the nodal values of the velocity of the solid and fluid phases are interpolated as follows:

$$\dot{\boldsymbol{\Psi}}(t) = \lambda_1 \dot{\boldsymbol{\Psi}}_n^+ + \lambda_2 \dot{\boldsymbol{\Psi}}_{n+1}^-, \quad \boldsymbol{W}(t) = \lambda_1 \boldsymbol{W}_n^+ + \lambda_2 \boldsymbol{W}_{n+1}^- \tag{68}$$

where $\lambda_1(t) = (t_{n+1} - t)/\Delta t$ and $\lambda_2(t) = (t - t_n)/\Delta t$, whereas

$$\dot{\boldsymbol{\Psi}}_n^{\pm} = \lim_{\varepsilon \to 0^{\pm}} \dot{\boldsymbol{\Psi}}(t_n + \varepsilon), \quad \boldsymbol{W}_n^{\pm} = \lim_{\varepsilon \to 0^{\pm}} \boldsymbol{W}(t_n + \varepsilon) \tag{69}$$

The same interpolation is assumed to hold for the nodal velocity of variation of the chemical potential of pore fluid too, namely

$$\dot{\boldsymbol{\Pi}}(t) = \lambda_1 \dot{\boldsymbol{\Pi}}_n^+ + \lambda_2 \dot{\boldsymbol{\Pi}}_{n+1}^- \quad \text{with } \dot{\boldsymbol{\Pi}}_n^{\pm} = \lim_{\varepsilon \to 0^{\pm}} \dot{\boldsymbol{\Pi}}(t_n + \varepsilon) \tag{70}$$

Note that the temporal jump in the functions $\dot{\boldsymbol{\Psi}}(t)$, $\boldsymbol{W}(t)$ and $\dot{\boldsymbol{\Pi}}(t)$ can be expressed as

$$[[\dot{\boldsymbol{\Psi}}_n]] = \dot{\boldsymbol{\Psi}}_n^+ - \dot{\boldsymbol{\Psi}}_n^-, \quad [[\boldsymbol{W}_n]] = \boldsymbol{W}_n^+ - \boldsymbol{W}_n^-, \quad [[\dot{\boldsymbol{\Pi}}_n]] = \dot{\boldsymbol{\Pi}}_n^+ - \dot{\boldsymbol{\Pi}}_n^- \tag{71}$$

The time integration of the velocity relationships leads to

$$\boldsymbol{\Psi}(t) = \boldsymbol{\Psi}_n + \frac{\lambda_2}{2}(\lambda_1 + 1)\Delta t \dot{\boldsymbol{\Psi}}_n^+ + \frac{\lambda_2^2}{2}\Delta t \dot{\boldsymbol{\Psi}}_{n+1}^- \tag{72}$$

$$\boldsymbol{\Pi}(t) = \boldsymbol{\Pi}_n + \frac{\lambda_2}{2}(\lambda_1 + 1)\Delta t \dot{\boldsymbol{\Pi}}_n^+ + \frac{\lambda_2^2}{2}\Delta t \dot{\boldsymbol{\Pi}}_{n+1}^- \tag{73}$$

which coincide with the third-order Hermite interpolation functions adopted by Li *et al.* [41].

Let $\mathscr{R}_s$ and $\mathscr{R}_w$ denote the residual vectors of the momentum balance equations of the whole porous medium (Equation (37)) and the pore fluid (Equation (38))

$$\mathscr{R}_i = \mathscr{R}_i^{\mathrm{dyn}}(\boldsymbol{\Psi}, \boldsymbol{\Pi}, \ddot{\boldsymbol{\Psi}}, \dot{\boldsymbol{W}}) + \mathscr{R}_i^{\mathrm{vis}}(\boldsymbol{\Psi}, \boldsymbol{\Pi}, \boldsymbol{W}, \dot{\boldsymbol{\Psi}}) + \mathscr{R}_i^{\mathrm{int}}(\boldsymbol{\Psi}, \boldsymbol{\Pi}) - \mathscr{R}_i^{\mathrm{ext}}(\mathscr{S}, \boldsymbol{\Psi}, \boldsymbol{\Pi}) = \mathscr{O} \tag{74}$$

where $i = s, w$ and $\mathscr{R}^{\mathrm{dyn}}$ is the vector containing inertial effects, $\mathscr{R}^{\mathrm{vis}}$ contains the viscous internal forces, $\mathscr{R}^{\mathrm{int}}$ contains the elastic internal forces and $\mathscr{R}^{\mathrm{ext}}$ contains the surface loadings (denoted collectively with $\mathscr{S}$) and the external body forces.

According to Chen *et al.* [65], the weak forms of Equations (74) after integration by parts of the inertial terms, is as follows:

$$\begin{aligned} &- \int_{t_n}^{t_{n+1}} \dot{\lambda} \mathscr{R}_i^{\mathrm{dyn}}(\boldsymbol{\Psi}, \boldsymbol{\Pi}, \dot{\boldsymbol{\Psi}}, \boldsymbol{W}) \mathrm{d}t + [\lambda \mathscr{R}_i^{\mathrm{dyn}}(\boldsymbol{\Psi}, \boldsymbol{\Pi}, \dot{\boldsymbol{\Psi}}, \boldsymbol{W})]_{t_n}^{t_{n+1}} \\ &+ \int_{t_n}^{t_{n+1}} \lambda [\mathscr{R}_i^{\mathrm{vis}}(\boldsymbol{\Psi}, \boldsymbol{\Pi}, \boldsymbol{W}, \dot{\boldsymbol{\Psi}}) + \mathscr{R}_i^{\mathrm{int}}(\boldsymbol{\Psi}, \boldsymbol{\Pi}) - \mathscr{R}_i^{\mathrm{ext}}(\mathscr{S}, \boldsymbol{\Psi}, \boldsymbol{\Pi})] \mathrm{d}t = \mathscr{O} \end{aligned} \tag{75}$$

DOI: 10.1002/nme

The weak form of the residual vectors of the mass balance equation of pore fluid (Equation (40)) is likewise

$$\int_{t_n}^{t_{n+1}} \lambda[\mathscr{R}_{\mu}^{\mathrm{vis}}(\boldsymbol{\Psi}, \boldsymbol{\Pi}, \boldsymbol{W}, \dot{\boldsymbol{\Psi}}, \dot{\boldsymbol{\Pi}})]\,\mathrm{d}t = \mathscr{O} \tag{76}$$

The weak forms represent a set of non-linear equations in the unknowns $\dot{\boldsymbol{\Psi}}_n^+$, $\dot{\boldsymbol{\Psi}}_{n+1}^-$, $\dot{\boldsymbol{\Pi}}_n^+$, $\dot{\boldsymbol{\Pi}}_{n+1}^-$, $\boldsymbol{W}_n^+$ and $\boldsymbol{W}_{n+1}^-$, the size of which is twice the size of the set obtained with classical finite difference schemes in time (e.g. the Newmark method), and which has been solved with the Newton–Raphson algorithm. The residuals equate to

$$\begin{aligned}\overline{\mathscr{R}}_{s1} = &-\int_{t_n}^{t_{n+1}} \dot{\lambda}_1 \mathscr{R}_s^{\mathrm{dyn}}(\boldsymbol{\Psi}, \boldsymbol{\Pi}, \dot{\boldsymbol{\Psi}}, \boldsymbol{W})\mathrm{d}t - \boldsymbol{M}_{11}(t_n)\dot{\boldsymbol{\Psi}}_n^- - \boldsymbol{M}_{12}(t_n)\boldsymbol{W}_n^- \\ &+ \int_{t_n}^{t_{n+1}} \lambda_1[\mathscr{R}_s^{\mathrm{vis}}(\boldsymbol{\Psi}, \boldsymbol{\Pi}, \boldsymbol{W}, \dot{\boldsymbol{\Psi}}) + \mathscr{R}_s^{\mathrm{int}}(\boldsymbol{\Psi}, \boldsymbol{\Pi}) - \mathscr{R}_s^{\mathrm{ext}}(\mathscr{S}, \boldsymbol{\Psi}, \boldsymbol{\Pi})]\,\mathrm{d}t \end{aligned} \tag{77}$$

$$\begin{aligned}\overline{\mathscr{R}}_{s2} = &-\int_{t_n}^{t_{n+1}} \dot{\lambda}_2 \mathscr{R}_s^{\mathrm{dyn}}(\boldsymbol{\Psi}, \boldsymbol{\Pi}, \dot{\boldsymbol{\Psi}}, \boldsymbol{W})\,\mathrm{d}t \\ &+ \int_{t_n}^{t_{n+1}} \lambda_2[\mathscr{R}_s^{\mathrm{vis}}(\boldsymbol{\Psi}, \boldsymbol{\Pi}, \boldsymbol{W}, \dot{\boldsymbol{\Psi}}) + \mathscr{R}_s^{\mathrm{int}}(\boldsymbol{\Psi}, \boldsymbol{\Pi}) - \mathscr{R}_s^{\mathrm{ext}}(\mathscr{S}, \boldsymbol{\Psi}, \boldsymbol{\Pi})]\,\mathrm{d}t \end{aligned} \tag{78}$$

$$\overline{\mathscr{R}}_{\mu 1} = \int_{t_n}^{t_{n+1}} \lambda_1[\mathscr{R}_{\mu}^{\mathrm{vis}}(\boldsymbol{\Psi}, \boldsymbol{\Pi}, \boldsymbol{W}, \dot{\boldsymbol{\Psi}}, \dot{\boldsymbol{\Pi}})]\,\mathrm{d}t \tag{79}$$

$$\overline{\mathscr{R}}_{\mu 2} = \int_{t_n}^{t_{n+1}} \lambda_2[\mathscr{R}_{\mu}^{\mathrm{vis}}(\boldsymbol{\Psi}, \boldsymbol{\Pi}, \boldsymbol{W}, \dot{\boldsymbol{\Psi}}, \dot{\boldsymbol{\Pi}})]\,\mathrm{d}t \tag{80}$$

$$\begin{aligned}\overline{\mathscr{R}}_{w1} = &-\int_{t_n}^{t_{n+1}} \dot{\lambda}_1 \mathscr{R}_w^{\mathrm{dyn}}(\boldsymbol{\Psi}, \boldsymbol{\Pi}, \dot{\boldsymbol{\Psi}}, \boldsymbol{W})\mathrm{d}t - \boldsymbol{M}_{21}(t_n)\dot{\boldsymbol{\Psi}}_n^- - \boldsymbol{M}_{22}(t_n)\boldsymbol{W}_n^- \\ &+ \int_{t_n}^{t_{n+1}} \lambda_1[\mathscr{R}_w^{\mathrm{vis}}(\boldsymbol{\Psi}, \boldsymbol{\Pi}, \boldsymbol{W}, \dot{\boldsymbol{\Psi}}) + \mathscr{R}_w^{\mathrm{int}}(\boldsymbol{\Psi}, \boldsymbol{\Pi}) - \mathscr{R}_w^{\mathrm{ext}}(\mathscr{S}, \boldsymbol{\Psi}, \boldsymbol{\Pi})]\,\mathrm{d}t \end{aligned} \tag{81}$$

$$\begin{aligned}\overline{\mathscr{R}}_{w2} = &-\int_{t_n}^{t_{n+1}} \dot{\lambda}_2 \mathscr{R}_w^{\mathrm{dyn}}(\boldsymbol{\Psi}, \boldsymbol{\Pi}, \dot{\boldsymbol{\Psi}}, \boldsymbol{W})\,\mathrm{d}t \\ &+ \int_{t_n}^{t_{n+1}} \lambda_2[\mathscr{R}_w^{\mathrm{vis}}(\boldsymbol{\Psi}, \boldsymbol{\Pi}, \boldsymbol{W}, \dot{\boldsymbol{\Psi}}) + \mathscr{R}_w^{\mathrm{int}}(\boldsymbol{\Psi}, \boldsymbol{\Pi}) - \mathscr{R}_w^{\mathrm{ext}}(\mathscr{S}, \boldsymbol{\Psi}, \boldsymbol{\Pi})]\,\mathrm{d}t \end{aligned} \tag{82}$$

Finally, it is worth noting that, in the case of linear problems in single-phase media, if a discontinuous displacement in time is assumed with linear shape functions in the time step, then the discontinuous Galerkin formulation given by Li and Wiberg [66] is recovered.

6. VERIFICATION OF THE FINITE ELEMENT PROCEDURES

The finite element formulation was verified with regard to fluid-saturated, neo-Hookean elastic material subjected to quasi-static loading and to dynamic 1D and 2D wave propagations. The numerical results are compared with semi-analytical results and with the analytical solutions available in the literature. A quasi-static loading was considered first to verify—for the first time—the numerical procedures when the mechanical coupling between the two phases is important, namely in undrained conditions (and therefore in the absence of inertial and viscous couplings), at large strains with compressible solid and fluid constituents.

DOI: 10.1002/nme

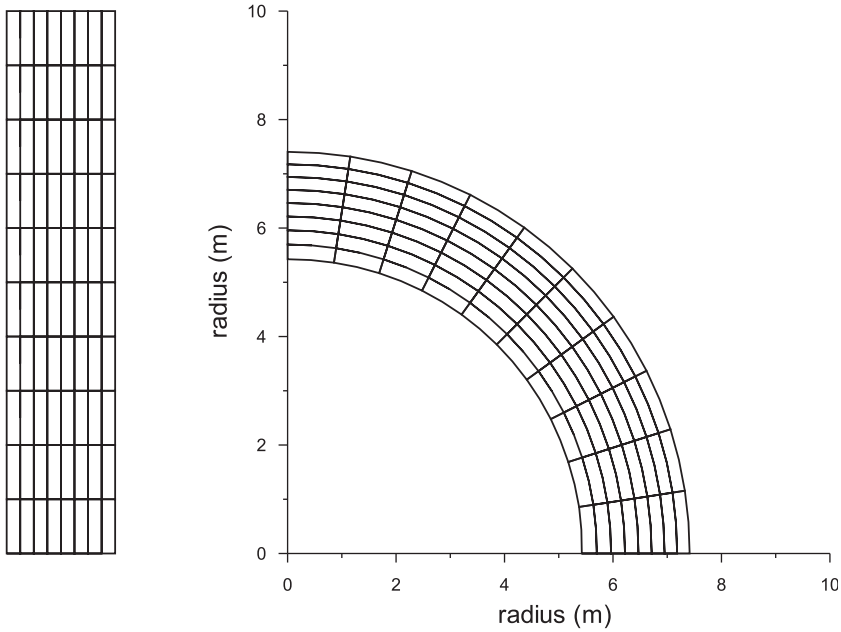

Figure 1. Undeformed (left) and deformed (right) finite element mesh for the finite bending of a compressible two-phase elastic block (with $\mathscr{K}/\mathscr{K}_s = 0.5$).

6.1. *Verification of the FEM for the finite bending of a compressible two-phase elastic block*

The plane strain, quasi-static flexure of a compressible, two-phase elastic block, rectangular in the undeformed configuration $l_0 \times h_0$, into a sector of a circular tube was considered first. This example is particularly interesting because the final geometry has been only partially specified, hence the validation concerns both the final stress state and the final configuration. A 'semi-analytical' solution for the plane strain problem is given in Appendix B. Although it was impossible to obtain an exact analytical solution, so that the momentum balance equations were integrated numerically, this solution will be denoted as *semi-analytical* below in order to distinguish it from the *numerical* solution obtained using the proposed finite element method (FEM). The results shown in this subsection were obtained with the simplified version of the finite element formulation because a quasi-static bending was analysed, but equivalent results can be obtained with the complete version of the finite element formulation.

Figure 1 shows the undeformed and the deformed mesh computed for $l_0 = 10$ m and $h_o = 2$ m, with the following constitutive parameters:

$$\mathscr{K} = 100.0\,\text{MPa}, \quad \mathscr{K}_s = 200.0\ \text{MPa}, \quad \mathscr{K}_w = 1000.0\,\text{MPa},$$
$$\mu = 140.0\,\text{MPa}, \quad n_0 = 0.50, \quad K_D^0 = 1 \times 10^{-9}\,\text{m/s},$$

thus the ratio of the bulk moduli is $\mathscr{K}/\mathscr{K}_s = 0.5$.

Taking advantage of the symmetries of the problem, just a quarter of a circular tube was analysed. The rectangular block was discretized with 80 finite elements. In the initial bending phases, fictitious constraints were considered on the shortest sides of the rectangular block. Then the fictitious constraints were progressively released until the final configuration was reached, in which no vertical and no horizontal displacements were specified on the horizontal and vertical faces, respectively (see Figure 1(b)). No flux of water through the external boundaries was permitted throughout the bending process. The very low permeability associated with the short flexure time (about 80 min) and the lack of drainage through the external boundaries give rise to an undrained condition.

DOI: 10.1002/nme

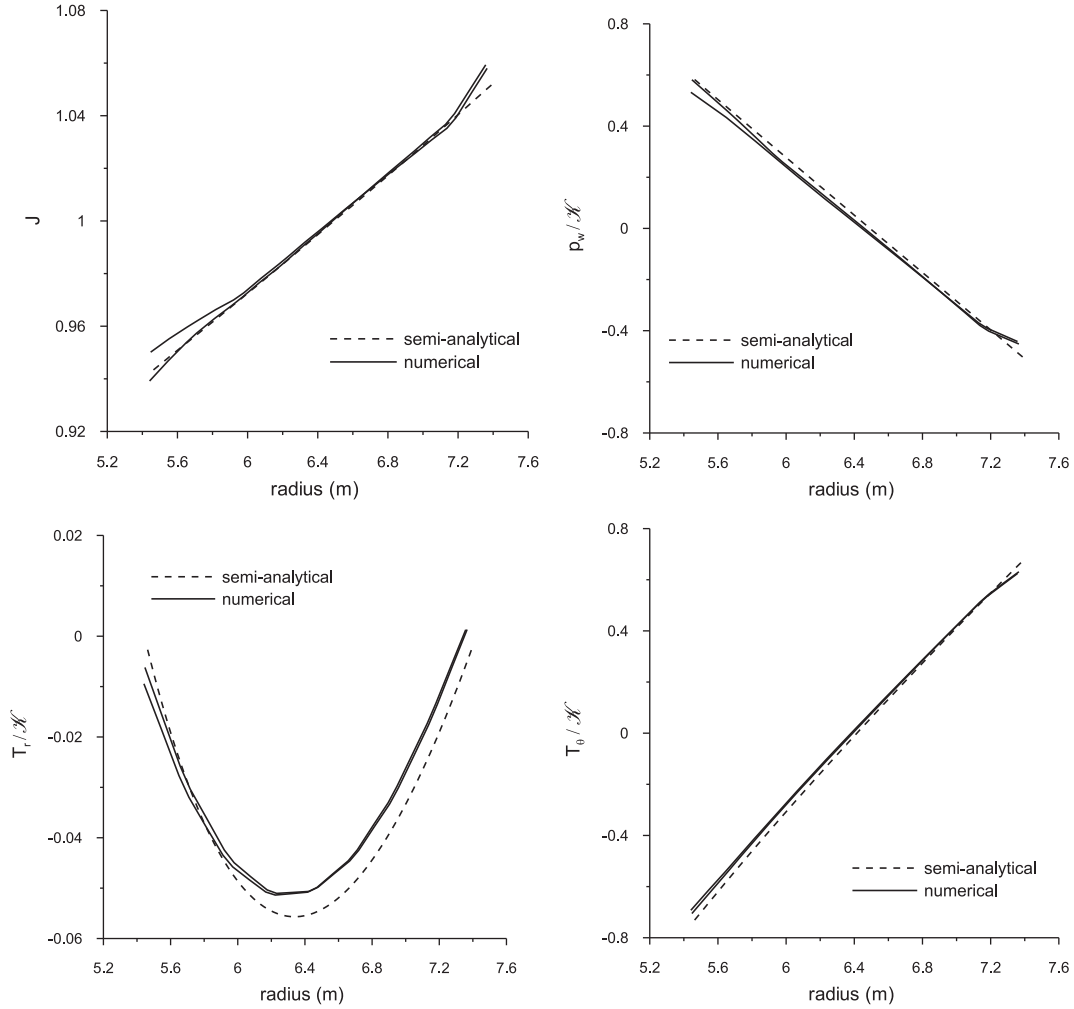

Figure 2. Comparison between numerical and semi-analytical results for the finite bending of a compressible two-phase elastic block with $\mathscr{K}/\mathscr{K}_s = 0.5$ under undrained conditions.

Figure 2 shows the comparison of the *semi-analytical* and *numerical* evaluations of J, the pore pressure p_w, and the radial and circumferential Cauchy stresses (T_r and T_θ, respectively), along the radius, which all showed an excellent agreement.

Figure 3 shows the effects induced by the compressibility of the solid constituent. The comparison is given for the case of an almost incompressible solid constituent ($\mathscr{K}_s = 1000.0\,\text{GPa}$, so $\mathscr{K}/\mathscr{K}_s = 1\times10^{-4}$) and the compressible case ($\mathscr{K}_s = 200.0\,\text{MPa}$, so $\mathscr{K}/\mathscr{K}_s = 0.5$). The *semi-analytical* results are not shown in this case for the sake of clarity, because the *semi-analytical* and *numerical* results have the same range of consistency as in Figure 2. Note in Figure 3 that the compressibility of the solid constituent leads to a larger pore pressure, p_w, and volume compression, J, whereas the effects on the radial Cauchy stress T_r and circumferential Cauchy stress T_θ are not shown because they are negligible.

Figure 4 shows the comparison of J and T_θ, computed considering a flexure under undrained conditions (with a compressible solid constituent, $\mathscr{K}/\mathscr{K}_s = 0.5$) with those obtained under drained conditions (which are equivalent to the flexure of a dry porous medium). Here again, the *semi-analytical* results are not shown for the sake of clarity, because their consistency with the *semi-analytical* results is excellent. The volume compression, J, is clearly much larger for the drained conditions, whereas T_θ is much smaller than in the undrained conditions.

DOI: 10.1002/nme

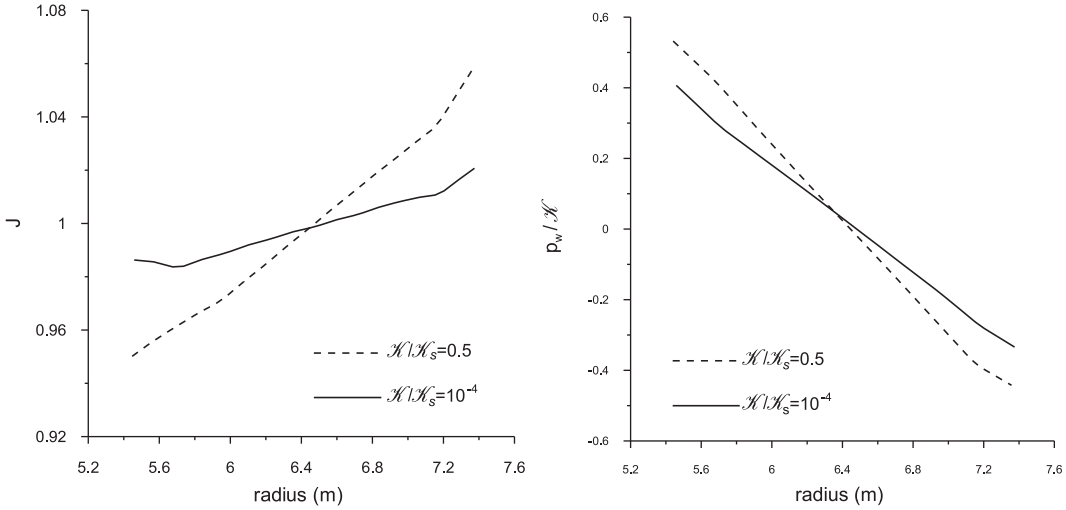

Figure 3. Comparison between the numerical results of the finite bending of a compressible two-phase elastic block obtained with $\mathscr{K}/\mathscr{K}_s = 0.5$ and $\mathscr{K}/\mathscr{K}_s = 1\times10^{-4}$ under undrained conditions.

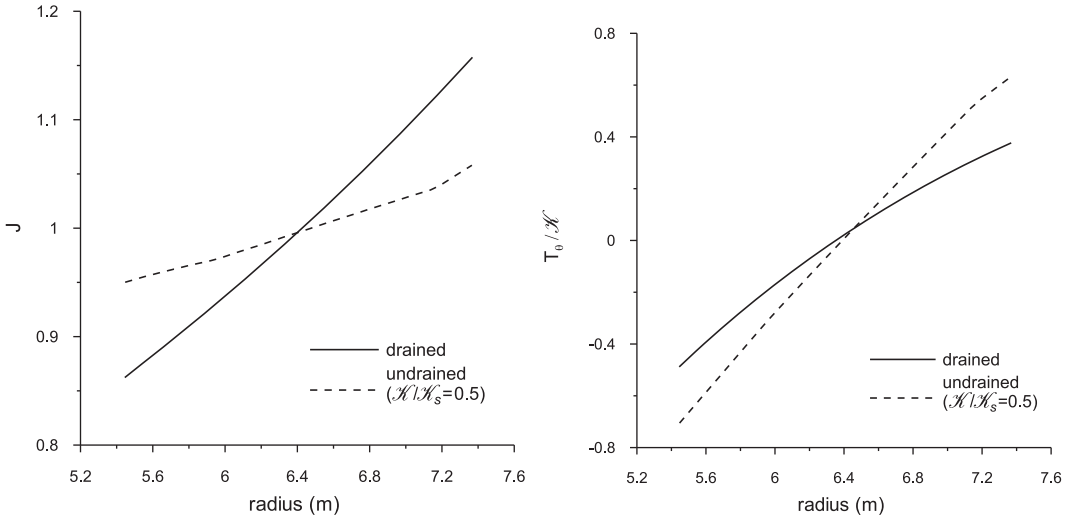

Figure 4. Comparison between numerical results for the finite bending of a compressible two-phase elastic block under undrained (with $\mathscr{K}/\mathscr{K}_s = 0.5$) and drained conditions.

Finally, Table I compares the values of the radius, r, and thickness, h, of the circular tube resulting from bending the compressible elastic block. The *numerical* results obtained with the proposed FEM are compared with the *semi-analytical* solution, in the cases of both undrained (with both compressible and incompressible solid constituents, $\mathscr{K}/\mathscr{K}_s = 0.5$ and $\mathscr{K}/\mathscr{K}_s = 1\times10^{-4}$) and drained flexure. It is worth noting that the discrepancies are greatest for undrained flexure when compressible solid constituents are considered ($\mathscr{K}/\mathscr{K}_s = 0.5$), i.e. <2 cm for the internal radius r (equivalent to 0.36 %) and <1 cm for the thickness h (equivalent to 0.5 %).

6.2. Verification of the FEM for 1D elastic wave propagation in a pre-stressed two-phase material

To verify the finite element procedures for dynamic problems, the propagation of a plane, longitudinal, small-amplitude elastic wave is investigated in two samples: the first is *unstrained* (so that the initial and final configurations coincide with each other) and the second has initially been

DOI: 10.1002/nme

Table I. Comparison of the numerical and semi-analytical values of the radius, r, and thickness, h, of the circular tube resulting from bending the compressible two-phase elastic block.

	Numerical results		Semi-analytical results	
Type of flexure	r(m)	h(m)	r(m)	h(m)
Undrained with $\mathscr{K}/\mathscr{K}_s = 0.5$	5.425	1.984	5.444	1.977
Undrained with $\mathscr{K}/\mathscr{K}_s = 1\times10^{-4}$	5.437	1.988	5.450	1.977
Drained	5.432	1.987	5.439	1.985

submitted to a large uniaxial, plane-strain, extension (so that the initial and final configurations are very different from one another) under drained conditions (i.e. slowly enough to keep pore pressure constant), and it is denoted as the *pre-strained* sample. The constitutive parameters of the two samples are very different from one another and are selected so that the longitudinal wave velocities of the samples in their final configurations are equal. Wave velocities must obviously coincide with the infinitesimal case, due to the small amplitude of the input pulse. Thus we can compare the numerical results with the analytical solution obtained by Gajo and Mongioví [18] for small-strain, longitudinal wave propagation in saturated porous media. The key point is that the final stiffness of the *pre-strained* sample is completely different from the initial value due to the large prestrain. The comparison with the analytical solution thus enables us to verify the numerical procedures when a small-amplitude wave travels in a completely deformed geometry, in which the stiffness has been completely changed by pre-straining. Only the results obtained with the complete finite element version (Section 5.1) are considered, because the simplified version (Section 5.2) is not reliable for wave propagation.

The constitutive parameters for the *pre-strained* sample were obtained assuming the same acoustic tensor coefficients for both samples (*unstrained* and *pre-strained*).

Considering the acceleration wave problem (where the velocity gradients and the accelerations are discontinuous), it can be demonstrated that, if $\boldsymbol{n}$ denotes the unit normal of the discontinuous surface in the current configuration, and the jump conditions are $[\![\boldsymbol{L}]\!]=\boldsymbol{g}^s\otimes\boldsymbol{n}$ and $[\![\mathrm{grad}\boldsymbol{w}]\!]=\boldsymbol{g}^w\otimes\boldsymbol{n}$, then the local jump conditions in the spatial settings lead to

$$\begin{bmatrix} \boldsymbol{A}+((1-n)\rho_s+n\rho_w)\omega^2\boldsymbol{I} & c(n\rho_w)\boldsymbol{n}\otimes\boldsymbol{n}+(n\rho_w)\omega^2\boldsymbol{I} \\ -c(n\rho_w)\boldsymbol{n}\otimes\boldsymbol{n}+(n\rho_w)\omega^2\boldsymbol{I} & -\mathrm{d}n\rho_w(n\rho_w J)\boldsymbol{n}\otimes\boldsymbol{n}+(n\rho_w\tau)\omega^2\boldsymbol{I} \end{bmatrix}\begin{bmatrix}\boldsymbol{g}^s\\ \boldsymbol{g}^w\end{bmatrix}=\begin{bmatrix}\boldsymbol{0}\\ \boldsymbol{0}\end{bmatrix} \tag{83}$$

where, in the special case of null pore pressure ($p_w=0$, thus $\mu_w=0$, $J_w=1$ and $J_{s-f}=1$), $c=-\beta\alpha J\mathscr{K}_w/m_w$ and

$$\boldsymbol{A}=\left(\frac{\mathscr{K}}{J}+\beta\mathscr{K}_w\frac{\alpha^2}{n}-\mathscr{K}\frac{\mathrm{Ln}J}{J}+\frac{5}{9}\mu J^{-5/3}\mathrm{tr}\boldsymbol{B}\right)\boldsymbol{n}\otimes\boldsymbol{n}$$

$$+(\mu J^{-5/3}(\boldsymbol{F}^{\mathrm{T}}\boldsymbol{n}\bullet\boldsymbol{F}^{\mathrm{T}}\boldsymbol{n}))\boldsymbol{I}-\tfrac{2}{3}\mu J^{-5/3}(\boldsymbol{n}\otimes\boldsymbol{B}\boldsymbol{n}+\boldsymbol{B}\boldsymbol{n}\otimes\boldsymbol{n}) \tag{84}$$

Equation (83) can be compared with the corresponding jump conditions for small strain theory, where the constitutive parameters for infinitesimal theory are denoted with a superposed tilde (˜)

$$\begin{bmatrix} \tilde{\boldsymbol{A}}+((1-n)\rho_s+n\rho_w)\omega^2\boldsymbol{I} & -(\tilde{\alpha}n\tilde{Q})\boldsymbol{n}\otimes\boldsymbol{n}+(n\rho_w)\omega^2\boldsymbol{I} \\ (\tilde{\alpha}n\tilde{Q})\boldsymbol{n}\otimes\boldsymbol{n}+(n\rho_w)\omega^2\boldsymbol{I} & -(n^2\tilde{Q})\boldsymbol{n}\otimes\boldsymbol{n}+(n\rho_w\tau)\omega^2\boldsymbol{I} \end{bmatrix}\begin{bmatrix}\boldsymbol{g}^s\\ \boldsymbol{g}^w\end{bmatrix}=\begin{bmatrix}\boldsymbol{0}\\ \boldsymbol{0}\end{bmatrix} \tag{85}$$

where

$$\tilde{\boldsymbol{A}}=\left(\tilde{\mathscr{K}}+\tilde{\alpha}^2\tilde{Q}+\tfrac{1}{3}\tilde{\mu}\right)\boldsymbol{n}\otimes\boldsymbol{n}+\tilde{\mu}\boldsymbol{I}$$

DOI: 10.1002/nme

Thus, from the comparison, $\tilde{Q}=d\rho_w^2 J=\beta\mathscr{K}_w/n$, which means that

$$\frac{1}{\tilde{Q}}=\frac{n}{\mathscr{K}_w}+\frac{(\alpha-n)J_s}{\mathscr{K}_s} \tag{86}$$

and

$$\tilde{\alpha}=\alpha=1-(J_s\mathscr{K})/(J\mathscr{K}_s) \tag{87}$$

$$\tilde{\mu}=\mu J^{-5/3}(\boldsymbol{F}^{\mathrm{T}}\boldsymbol{n}\bullet\boldsymbol{F}^{\mathrm{T}}\boldsymbol{n}) \tag{88}$$

Finally, in the special case where

$$\boldsymbol{F}=\begin{bmatrix} F_{11} & 0 & 0 \\ 0 & F_{22} & 0 \\ 0 & 0 & 1 \end{bmatrix}$$

and $\boldsymbol{n}=[0\ \ 1\ \ 0]^{\mathrm{T}}$, thus $J=F_{11}F_{22}$, $\boldsymbol{Bn}=F_{22}^2\boldsymbol{n}$ and $(\boldsymbol{F}^{\mathrm{T}}\boldsymbol{n}\bullet\boldsymbol{F}^{\mathrm{T}}\boldsymbol{n})=F_{22}^2$, then

$$\tilde{\mathscr{K}}=\frac{\mathscr{K}}{J}-\mathscr{K}\frac{\mathrm{Ln}J}{J}+\frac{5}{9}\mu J^{-5/3}(F_{11}^2+F_{22}^2+1)-\frac{5}{3}\mu J^{-5/3}F_{22}^2 \tag{89}$$

In the case of small displacements and strains, $J\approx 1+\varepsilon$ (with $\varepsilon=\mathrm{tr}\epsilon$ and ϵ the linearized strain tensor), $\mathrm{Ln}J\approx\varepsilon$, $\mathrm{Ln}J_{s-f}\approx\varepsilon_{s-f}$ (with $\varepsilon_{s-f}=-p_w/\mathscr{K}_s$), $F_{11}^2+F_{22}^2+1\approx 3+2\varepsilon_{11}+2\varepsilon_{22}$, $F_{22}^2\approx 1+2\varepsilon_{22}$, the parameters with a superposed ($\tilde{}$) obviously coincide with those with no ($\tilde{}$).

Analytical results for harmonic wave propagation in saturated porous media for small strains are available for instance for the following constitutive parameters:

$$\begin{aligned} &\tilde{\mathscr{K}}=1000\text{ MPa}, \quad \tilde{\mathscr{K}}_s=36000\text{ MPa}, \quad \tilde{\mathscr{K}}_w=2177\text{ MPa}, \\ &\tilde{\mu}=461.54\text{ MPa}, \quad \rho_s=2700\,\mathrm{kg/m^3}, \quad \rho_w=1000\,\mathrm{kg/m^3}, \\ &\tau=1, \quad n=0.4 \end{aligned} \tag{90}$$

These parameters give $\tilde{Q}=5009.16\,\mathrm{MPa}$ and $\tilde{\alpha}=0.9722$, and consequently lead to the following wave velocities: 1852.28 and 763.11 m/s for the longitudinal waves of the first and second kind, respectively, in the case of null viscous coupling, and 1773.03 m/s for the longitudinal wave in the case of very large viscous coupling. This set of constitutive parameters was adopted for the first (i.e. the *unstrained*) sample.

Equations (86)–(89) enable us to evaluate the constitutive parameters of the second *pre-strained* sample so as to have the same wave velocities as in the first *unstrained* sample. If the second sample is stretched under plain strain conditions to $F_{22}=2$ and $F_{11}=0.55564$ (thus $K_{11}=0$, $K_{\mathrm{vol}}=187.32\,\mathrm{MPa}$ and $J=1.1113$), the constitutive parameters must equate to

$$\begin{aligned} &\mathscr{K}=1775.26\text{ MPa}, \quad \mathscr{K}_s=57791.2\,\mathrm{MPa}, \quad \mathscr{K}_w=2108.76\text{ MPa}, \\ &\mu=137.57\text{ MPa}, \quad \rho_{s0}=2713.22\,\mathrm{kg/m^3}, \quad \rho_{w0}=1000.0\,\mathrm{kg/m^3}, \\ &\tau=1, \quad n_0=0.33648 \end{aligned} \tag{91}$$

The following meaningful values of hydraulic conductivity have been selected because they are representative of three well-defined types of propagation of the longitudinal waves in a propagation length of 1 cm: $\tilde{K}_D=10^{-1}$, $\tilde{K}_D=10^{-5}$, $\tilde{K}_D=10^{-9}\,\mathrm{m/s}$, which represent low, intermediate and high viscous coupling, respectively, in the small strain analysis.

It is generally well accepted that the scaling of the hydraulic conductivity is given in Equation (12), hence

$$\boldsymbol{K}_D=\frac{1}{J}\boldsymbol{F}\boldsymbol{K}_D^0\boldsymbol{F}^{\mathrm{T}} \tag{92}$$

DOI: 10.1002/nme

where $\boldsymbol{K}_D$ is the second-order tensor defining the hydraulic conductivity in the deformed configuration and $\boldsymbol{K}_D^0$ defines the scaled quantity in the reference configuration. Thus in the case of isotropy $\boldsymbol{K}_D^0 = K_D^0 \boldsymbol{I}$, from an assigned hydraulic conductivity in the current configuration $(K_D)_{22} = \tilde{K}_D$, the hydraulic conductivity in the reference configuration is $K_D^0 = (K_D)_{22} F_{11}/F_{22}$, namely (in our case): $K_D^0 = 0.278 \times 10^{-1}$, $K_D^0 = 0.278 \times 10^{-5}$ and $K_D^0 = 0.278 \times 10^{-9}$ m/s.

The *unstrained* sample (with the constitutive parameters given in Equation (90)) has an initial geometry of 2 cm in height and 0.55564 cm in width. The *pre-strained* sample has an initial geometry (i.e. before pre-straining) of 1 cm in height and 1 cm in width, and the constitutive parameters given in Equation (91). Denoting the vertical direction with 2 and the in-plane, horizontal direction with 1, the second sample was first pre-strained to $F_{22} = 2$ and $F_{11} = 0.55564$, so that its final geometry coincided with the initial geometry of the first sample, and the equivalence of the acoustic tensors was expected to give the same velocities of longitudinal wave propagation in the two samples.

Both samples were discretized with 100 finite elements. The temporal integration involved steps of 0.05 μs, roughly corresponding to the time it took the fastest wave to move between two adjacent nodes in the current configuration. The adopted input pulse consists in a smooth step displacement $(-1 \times 10^{-6}$ m) boundary condition applied to the solid phase at the upper boundary of the sample, with a null relative fluid velocity (hence the displacement boundary condition applied to the fluid phase equates that of the solid phase), which is associated with an unknown pore pressure. To prevent extremely short wavelengths in the simulations, the Heaviside function was regularized by considering a half period of a *cosine* function of period 2 μs (so the rise phase takes 1 μs). This implies that the rise phase of the fastest-travelling wave involves about five finite elements or 10 nodes) and should consequently be well represented by the finite element mesh adopted.

Lateral horizontal solid displacements and fluid velocities were prevented during wave propagation, so as to simulate the longitudinal wave propagation in a semi-finite stratum. Note that, in the initial phase of pre-straining of the second sample, the horizontal solid displacements were permitted with no horizontal lateral fluid velocities. In both samples and for all loading phases, drainage was permitted at the bottom boundary by imposing a null pore pressure, which is associated with unknown relative fluid velocities.

Figure 5 shows the solid displacement history after the longitudinal wave had travelled 1 cm. The theoretical and numerical results are compared: the theoretical results were obtained by means of a numerical convolution of the analytical solution provided by Gajo and Mongioví [18] for a step boundary condition (the Heaviside function); the numerical results obtained on the *unstrained* sample coincided perfectly with the results obtained on the *pre-strained* sample, as expected from the equivalence of the acoustic tensors. The finite element solution was clearly consistent with the analytical results and correctly reproduced the main aspects of the propagating wave, both in the extreme conditions of permeability (two waves for $\tilde{K}_D = 10^{-1}$ m/s and only one wave for $\tilde{K}_D = 10^{-9}$ m/s) and in the intermediate condition of permeability ($\tilde{K}_D = 10^{-5}$ m/s). Like the finite element methods investigated by Gajo *et al.* [22] for the dynamic behaviour of saturated porous media under small strains, the finite element procedure proposed here for geometrical and material non-linear effects is perfectly adequate for dealing with the dispersive characteristics of wave propagation in porous media, i.e. with the fact that each frequency component propagates with its own velocity.

It is well known, however, that the Newmark scheme is not suitable for the analysis of step-wise wave propagation, because spurious oscillations are evident in the numerical solutions. The numerical response can be improved by using discontinuous Galerkin finite elements in the time domain. Figure 6 shows the comparison between the theoretical and numerical solid displacements, whereas Figure 7 shows the comparison for the fluid displacements (denoted with U); the latter were obtained using a numerical integration of the nodal values, namely

$$U_2 = \Psi_2 + W_2 \Delta t$$

The comparison of Figures 5 and 6 shows the different effectiveness of the discontinuous Galerkin method on the longitudinal waves of the first and second time, respectively. This kind

DOI: 10.1002/nme

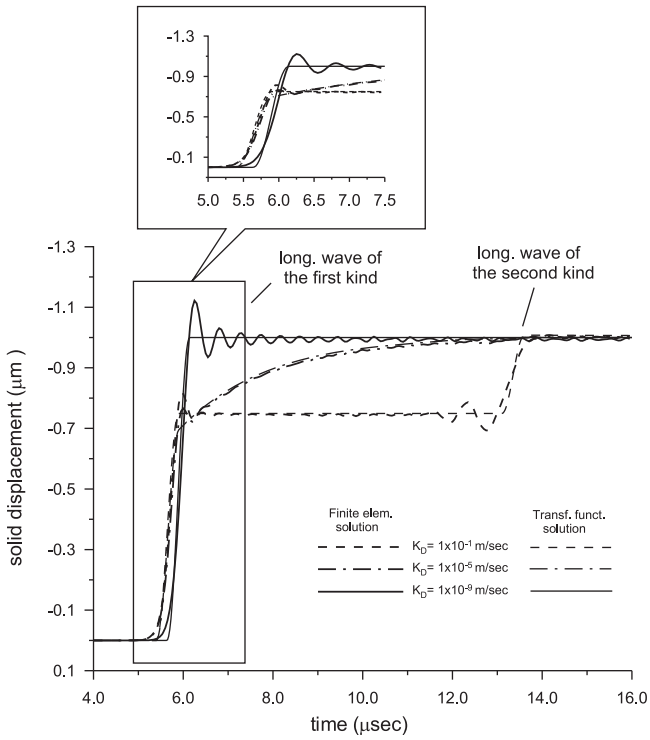

Figure 5. Solid displacement history at 1 cm, for different values of $\tilde{K}_D$. Comparison between theoretical and numerical results obtained with Newmark time integration algorithm.

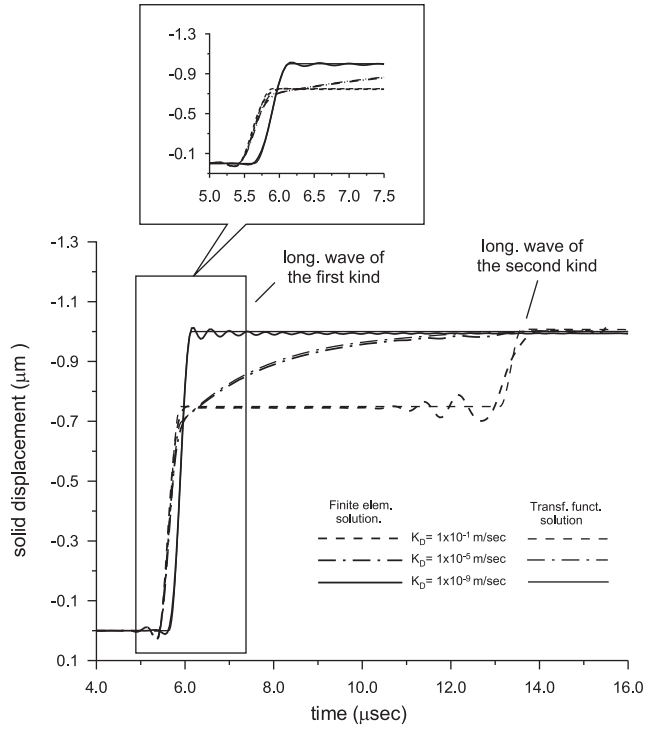

Figure 6. Solid displacement history at 1 cm, for different values of $\tilde{K}_D$. Comparison between theoretical and numerical results obtained with discontinuous Galerkin finite elements in the time domain.

DOI: 10.1002/nme

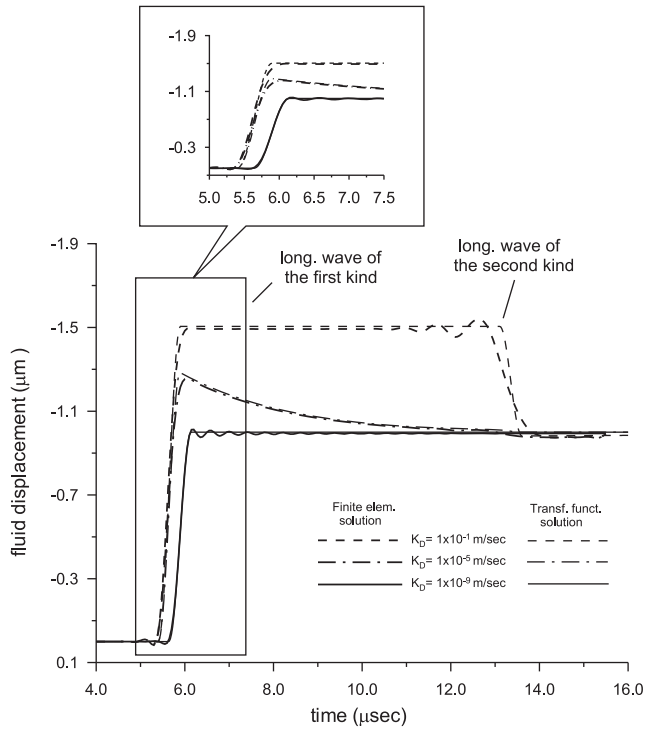

Figure 7. Fluid displacement history at 1 cm, for different values of $\tilde{K}_D$. Comparison between theoretical and numerical results obtained with discontinuous Galerkin finite elements in the time domain.

of comparison has never been performed before, to the best of the Authors' knowledge. It can be observed that the discontinuous FEM is effective in reducing the spurious oscillations related to the arrival of the first longitudinal wave, whereas it is scarcely effective for the spurious oscillations related to the second wave (see the case of $\tilde{K}_D = 10^{-1}$ m/s).

Finally, for the sake of completeness, Figure 8 shows the computed pore pressure history for different values of $\tilde{K}_D$.

6.3. Verification of the FEM for 2D elastic wave propagation in a pre-stressed two-phase material

The finite element procedures for dynamic problems were also validated for the 2D propagation of a non-planar, small-amplitude elastic wave in a sample that had previously been submitted to a large isotropic compression, where $F_{11} = F_{22} = 0.5$ (and $F_{33} = 1$, due to plane strain conditions). The validation test selected is representative of the dynamic tests typically performed on laboratory samples using piezoelectric transducers. The constitutive parameters are as follows:

$$\begin{aligned} &\mathscr{K} = 131.63 \text{ MPa}, \quad \mathscr{K}_s = 17761.5 \text{ MPa}, \quad \mathscr{K}_w = 2306.06 \text{ MPa}, \\ &\mu = 183.16 \text{ MPa}, \quad \rho_{s0} = 2532.1 \text{kg/m}^3, \quad \rho_{w0} = 1000.0 \text{kg/m}^3, \\ &\tau = 1, \quad n_0 = 0.84 \end{aligned} \tag{93}$$

The constitutive parameters describing the small-strain wave propagation in the deformed sample were evaluated following the procedure described in the previous section, and were found to amount to

$$\begin{aligned} &\tilde{\mathscr{K}} = 2025.7 \text{ MPa}, \quad \tilde{\mathscr{K}}_s = 72865.5 \text{ MPa}, \quad \tilde{\mathscr{K}}_w = 2043.5 \text{ MPa}, \\ &\tilde{\mu} = 461.54 \text{ MPa}, \quad \rho_s = 2700 \text{kg/m}^3, \quad \rho_w = 1000 \text{kg/m}^3, \\ &\tau = 1, \quad n = 0.4 \end{aligned} \tag{94}$$

DOI: 10.1002/nme

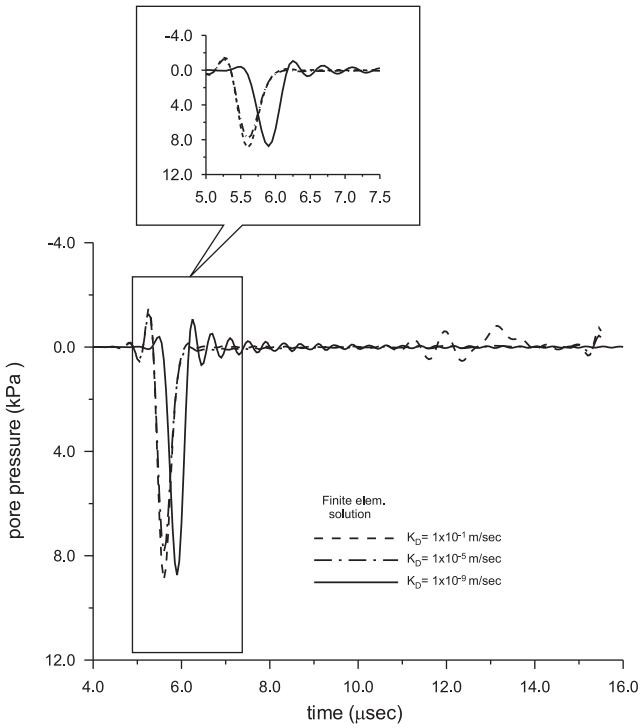

Figure 8. Pore pressure history at 1 cm, for different values of $\tilde{K}_D$. The numerical results were obtained with discontinuous Galerkin finite elements in the time domain.

The latter parameters characterize the behaviour of a second sample (that had not been prestrained), which has the same wave velocities as the prestrained sample. The constitutive parameters give $\tilde{Q} = 4911.6\,\text{MPa}$ and $\tilde{\alpha} = 0.9722$, and consequently lead to the following small-strain wave velocities (in the deformed configuration): 1930.95 and 926.84 m/s for the longitudinal waves of the first and second kind, respectively, in the case of null viscous coupling, and 1898.85 m/s for the longitudinal wave in the case of very large viscous coupling. The expected rotational wave velocities are 533.8 and 478.0 m/s in the cases of null and very large viscous coupling, respectively.

In the case of low permeability (namely very large viscous coupling), any relative motion between the phases is prevented, so that the porous material behaves like a single-phase medium, for which some analytical solutions are available. In order to have the same longitudinal and rotational wave velocities in the single-phase material as in the low-permeable saturated porous medium (namely 1898.85 and 478.0 m/s), the elastic properties of the single-phase medium must be $\mu = 461.54\,\text{MPa}$ and $\mathscr{K} = 6667.6\,\text{MPa}$, with $\rho = 2020\,\text{kg/m}^3$. The selected analytical solution is that proposed by Eason *et al.* [67], for a suddenly applied line load in an unbounded medium, which can be reformulated as a boundary value problem for a half-space with null horizontal displacements at the surface (from the antisymmetry of the line load in the unbounded medium).

The following geometrical properties were considered: the initial geometry of the sample is a rectangle 8 cm high and 16 cm wide. After isotropic compression (in plane strain conditions), the new sample dimensions are 4 and 8 cm, respectively (Figure 9). The applied input pulse consists of a vertical traction with an amplitude of 1 MPa (on the deformed configuration) applied on the upper surface of the sample, over a width of 2 cm, and varying as a single sine pulse of period 100 μs. Taking advantage of the symmetry of the problem, only half the sample was discretized with 16×16 finite elements, involving 1089 nodes with nearly 5000 degrees of freedom. Time integration was only performed with the Newmark algorithm, using time steps of 0.2 μs. It is worth noting that the spatial discretization enables an appropriate representation of the travelling pulse, which has a wave length of about 2 cm (as far as the longitudinal component is concerned)

DOI: 10.1002/nme

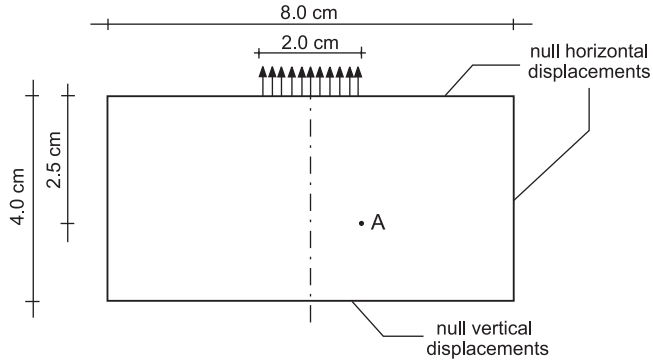

Figure 9. Final geometry and boundary conditions for the 2D wave propagation test.

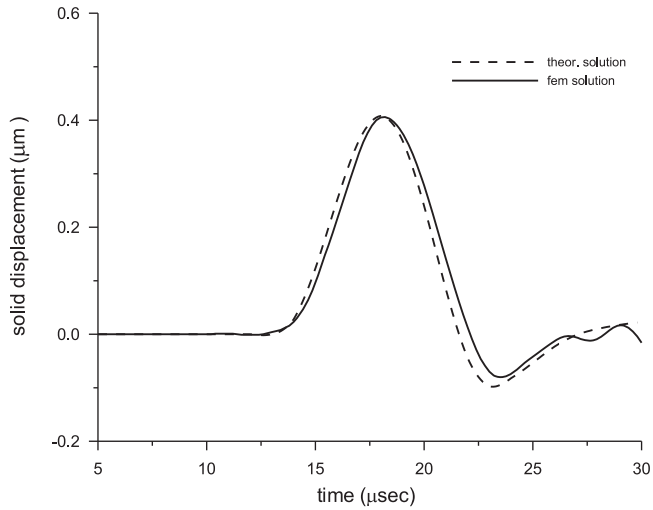

Figure 10. Solid displacement history at point A of Figure 9, for $\tilde{K}_D = 10^{-9}$ m/s. Comparison between theoretical and numerical results obtained with the Newmark time integration algorithm.

involving about 15 nodes. The boundary conditions applied to the sample and the position of the point A (where the transit of the input pulse is analysed), are shown in Figure 9. Note that the position of the point A was selected so as to avoid spurious reflected waves from the external boundaries of the sample.

Figure 10 shows the comparison of the vertical displacements of the solid skeleton computed by using the proposed FEM with the theoretical evaluations obtained by means of a numerical convolution and a spatial integration (over the length of 2 cm) of the analytical solution provided by Eason *et al.* [67], using the algorithms offered by Mathematica. The numerical results are obtained with $\tilde{K}_D = 10^{-9}$ m/s. The agreement is very good, although the numerical algorithms seem to evaluate a slightly slower propagation velocity.

Finally, for the sake of completeness, Figure 11 shows the effects of permeability on the history of vertical displacements at point A of Figure 9: the higher the permeability, the smaller the amplitude of the first longitudinal wave in terms of solid displacements (this is also consistent with Figure 6). Moreover, the arrival of the second longitudinal wave is observed in the case where the permeability is the highest ($\tilde{K}_D = 10^{-1}$ m/s).

Note in Figures 10 and 11 that the Newmark algorithm is resulted fairly efficient in capturing the propagation of the impulse wave generated by a single sine pulse and the discontinuous Galerkin method was not necessary in this case.

DOI: 10.1002/nme

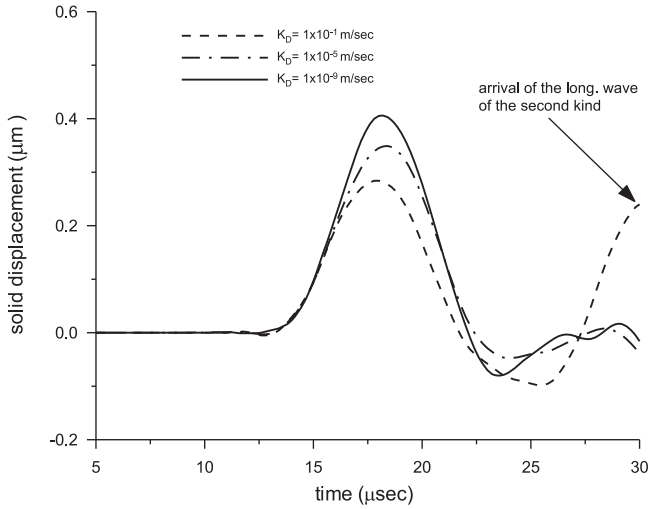

Figure 11. Solid displacement history at point A of Figure 9, for different values of $\tilde{K}_D$. The numerical results have been obtained with the Newmark time integration algorithm.

7. CONCLUSIONS

This paper is the first to provide a finite element solution for the dynamic behaviour of saturated porous media in the case of compressible fluid and solid constituents, including geometrical and material non-linear effects both in the solid and fluid constituents (i.e. at the microscale) and in the solid skeleton (i.e. at the macroscale).

The first part of the paper briefly recalls the mass and momentum balance equations for a saturated porous medium with compressible constituents, considering the material setting (whereas the balance equations for the spatial setting are recalled in Appendix A). Reference is made to the hyperelastic framework recently provided by Gajo [38] in the case of compressible constituents and non-linear geometrical effects. Thus, in the material setting, the stress-like quantities are the first Piola–Kirchhoff stress tensor $\boldsymbol{S}$ and the chemical potential of the pore fluid μ_w, while the work-conjugated, strain-like quantities are the deformation gradient $\boldsymbol{F}$ and the variation of fluid mass content $\bar{m}_w$. The momentum and mass balance equations for the pore fluid are expressed for the first time in terms of the chemical potential and the mass flux of the pore fluid, in order to take the compressibility of the fluid properly into account.

Finally, the governing equations for the material setting are expressed in two different weak forms, which enable the application of the FEM. The first weak form consists of a three-field formulation (namely the solid displacement, the relative fluid velocity and the pore fluid chemical potential), which is suitable for high-frequency dynamic problems. In this case, to avoid considering a further unknown field, the nodal mass fluxes are deduced in a weak form from the nodal relative velocities of the pore fluid. The second weak form consists of a two-field formulation (namely the solid displacement and the pore fluid chemical potential), which is a simplification of the first, in which some inertial effects of the pore fluid are neglected. The second formulation is consequently suitable for the analysis of problems in which the frequency components are not excessively high. The two formulations are the direct extension to non-linear geometrical problems with compressible constituents of the well-known $\boldsymbol{u}-\boldsymbol{w}-p$ and $\boldsymbol{u}-p$ formulations for the small-strain analysis of saturated porous media [21, 22].

The reliability of the proposed FEMs emerges clearly from the comparison of the numerical results with the analytical and semi-analytical solutions proposed in the literature, or developed in this work, relating to both quasi-static and dynamic 1D and 2D problems. The three-field formulation, in particular, proved perfectly adequate for dealing with the dispersive characteristics of wave propagation in porous media.

DOI: 10.1002/nme

This work thus paves the way to future developments in the study of non-isothermal behaviour and chemo-mechanical coupling in multiphase porous media with compressible constituents and non-linear effects.

APPENDIX A: BALANCE EQUATIONS IN THE CURRENT CONFIGURATION

From Equation (10) and from the identity $\mathrm{Grad}\mu_w = \boldsymbol{F}^{\mathrm{T}}\mathrm{grad}\mu_w$ we know that the *Cauchy* mass flux is equal to

$$\boldsymbol{M} = -\rho_w \frac{K_D^0}{g}\frac{1}{J}\boldsymbol{B}\mathrm{grad}(\mu_w + U) \tag{A1}$$

Equation (A1) highlights the change in hydraulic conductivity (involving hydraulic anisotropy) induced by the large strain of the solid phase.

The mass balance equation in the current configuration $\mathscr{B}$ becomes

$$\dot{\tilde{m}}_w = -J\,\mathrm{div}\boldsymbol{M} \tag{A2}$$

It is worth noting that the definition of *Cauchy* and *Piola–Kirchhoff* mass fluxes given in Equations (A1) and (10) corresponds to the heat fluxes in thermal problems (e.g. [68–71]).

For an element volume moving with the solid phase, the momentum balance equation for the whole porous medium in the current configuration $\mathscr{B}$ is

$$(1-n)\rho_s\dot{\boldsymbol{v}}_s + \frac{1}{J}[n\rho_w J(\boldsymbol{v}_s + \boldsymbol{w})]^{\cdot} = -\mathrm{div}[(\boldsymbol{v}_s + \boldsymbol{w})\otimes\boldsymbol{M}] + \mathrm{div}\boldsymbol{T} + [(1-n)\rho_s + n\rho_w] \tag{A3}$$

where $\boldsymbol{b} = \boldsymbol{b}_0/J$ is the body force per unit mass in the current configuration and $\boldsymbol{T}$ is the *total* Cauchy stress tensor (which is related to the *total* Kirchhoff stress tensor $\boldsymbol{K}$ through $\boldsymbol{K} = J\boldsymbol{T}$).

From Equations (A2) and (9), the rate of increase in momentum per unit of initial volume in the current configuration can be expressed as follows:

$$\frac{1}{J}[n\rho_w J(\boldsymbol{v}_s + \boldsymbol{w})]^{\cdot} = n\rho_w(\dot{\boldsymbol{v}}_s + \dot{\boldsymbol{w}}) - (\mathrm{div}\boldsymbol{M})(\boldsymbol{v}_s + \boldsymbol{w}) \tag{A4}$$

Moreover, since

$$\mathrm{div}\,[(\boldsymbol{v}_s + \boldsymbol{w})\otimes\boldsymbol{M}] = (\mathrm{div}\boldsymbol{M})\,(\boldsymbol{v}_s + \boldsymbol{w}) + \mathrm{grad}(\boldsymbol{v}_s + \boldsymbol{w})\boldsymbol{M} \tag{A5}$$

and taking into account Equation (7) and the fact that the gradient of the velocity field is $\boldsymbol{L} = \mathrm{grad}\boldsymbol{v}_s = \dot{\boldsymbol{F}}\boldsymbol{F}^{-1}$, then the momentum balance equation in the current configuration is reduced to

$$(1-n)\rho_s\dot{\boldsymbol{v}}_s + n\rho_w(\dot{\boldsymbol{v}}_s + \dot{\boldsymbol{w}}) = -n\rho_w(\dot{\boldsymbol{F}}\boldsymbol{F}^{-1} + \mathrm{grad}\boldsymbol{w})\boldsymbol{w} + \mathrm{div}\boldsymbol{T} + [(1-n)\rho_s + n\rho_w]\boldsymbol{b} \tag{A6}$$

The term $n\rho_w(\dot{\boldsymbol{F}}\boldsymbol{F}^{-1} + \mathrm{grad}\boldsymbol{w})\boldsymbol{w}$ in Equation (A6) represents the convective fluid acceleration force.

The momentum balance equation for the pore fluid in the current configuration $\mathscr{B}$ is

$$n\rho_w(\dot{\boldsymbol{v}}_s + \dot{\boldsymbol{w}}) = -n\rho_w(\dot{\boldsymbol{F}}\boldsymbol{F}^{-1} + \mathrm{grad}\boldsymbol{w})\boldsymbol{w} + n\mathrm{div}(-p_w\boldsymbol{I}) + \boldsymbol{f}_w + n\rho_w\boldsymbol{b} \tag{A7}$$

where the momentum supply $\boldsymbol{f}_w$ (per unit of volume in $\mathscr{B}$) is a volume force scaling in the same way as the other volume forces, so in the current configuration

$$\boldsymbol{f}_w = \boldsymbol{f}_{w0}/J \tag{A8}$$

and from Equation (20)

$$\boldsymbol{f}_w = -n\frac{g}{K_D^0}J\boldsymbol{B}^{-1}(\overbrace{n\rho_w\boldsymbol{w}}^{\boldsymbol{M}}) - \rho_a\dot{\boldsymbol{w}} \tag{A9}$$

DOI: 10.1002/nme

Noting, from Equation (13), that $\mathrm{div}(-p_w\boldsymbol{I})=-\rho_w\,\mathrm{grad}\mu_w$, in the case of permanent pore flow (thus $\dot{\boldsymbol{v}}_s=\boldsymbol{0}$ and $\dot{\boldsymbol{w}}=\boldsymbol{0}$) and negligible convective terms, then Equation (A7) is reduced to Equation (A1).

Equation (A7) can thus be rewritten as

$$n\rho_w(\dot{\boldsymbol{v}}_s+\tau\dot{\boldsymbol{w}})=-n\rho_w(\dot{\boldsymbol{F}}\boldsymbol{F}^{-1}+\mathrm{grad}\boldsymbol{w})\boldsymbol{w}-n\rho_w\mathrm{grad}\mu_w-n\frac{g}{K_D^0}J\boldsymbol{B}^{-1}\boldsymbol{M}+n\rho_w\boldsymbol{b} \tag{A10}$$

APPENDIX B: FINITE BENDING OF A COMPRESSIBLE TWO-PHASE ELASTIC BLOCK

The analytical solution of the plane strain flexure of an incompressible elastic block, rectangular in the undeformed configuration $l_0\times h_0$, into a sector of a circular tube was proposed by Green and Zerna [72], while the compressible case was provided by Ogden [73]. No analytical solution is available for two-phase media.

Let X_1, X_2 and X_3 (where $X_1\in[-h_0/2,h_0/2]$, $X_2\in[-l_0/2,l_0/2]$ and X_3 in the out of plane direction) denote the Cartesian coordinates in the undeformed configuration $\mathscr{B}_0$ and $\boldsymbol{E}_1,\boldsymbol{E}_2,\boldsymbol{E}_3$ the corresponding unit vectors.

Let us introduce an intermediate configuration $\mathscr{B}_{\mathrm{int}}$ in which the elastic block is still rectangular $\overline{l}_0\times\overline{h}_0$ (with $\overline{l}_0=l_0$), with Cartesian coordinates $\overline{X}_1,\overline{X}_2,\overline{X}_3$ (where $\overline{X}_1\in[0,\overline{h}_0]$, $\overline{X}_2\in[-l_0/2,l_0/2]$ and $\overline{X}_3$ is in the out-of-plane direction) and corresponding unit vectors $\overline{\boldsymbol{E}}_1,\overline{\boldsymbol{E}}_2,\overline{\boldsymbol{E}}_3$.

Finally the deformed configuration $\mathscr{B}$ is a sector of a cylindrical tube with semi-angle $\overline{\theta}$, thickness h and inner radius r_i. It is instrumental to adopt cylindrical coordinates $r\in[r_i,r_e]$, $\theta\in[-\overline{\theta},\overline{\theta}]$ and z (z is along the out-of-plane direction). Let $\mathbf{e}_r$, $\mathbf{e}_\theta$ and $\mathbf{e}_z$ be the corresponding unit vectors.

The deformation is described by the following relationships:

$$\overline{X}_1=v(X_1),\quad \overline{X}_2=X_2,\quad \overline{X}_3=X_3 \tag{B1}$$

and

$$r=f(\overline{X}_1),\quad \theta=g(\overline{X}_2),\quad z=\overline{X}_3 \tag{B2}$$

where the three functions v, f and g are unknown for the time being. The deformation gradient from $\mathscr{B}_0$ to $\mathscr{B}_{\mathrm{int}}$ is

$$\boldsymbol{F}_1=v'\overline{\boldsymbol{E}}_1\otimes\boldsymbol{E}_1+\overline{\boldsymbol{E}}_2\otimes\boldsymbol{E}_2+\overline{\boldsymbol{E}}_3\otimes\boldsymbol{E}_3 \tag{B3}$$

whereas the deformation gradient from $\mathscr{B}_{\mathrm{int}}$ to $\mathscr{B}$ is

$$\boldsymbol{F}_2=f'\mathbf{e}_r\otimes\overline{\boldsymbol{E}}_1+fg'\mathbf{e}_\theta\otimes\overline{\boldsymbol{E}}_2+\mathbf{e}_z\otimes\overline{\boldsymbol{E}}_3 \tag{B4}$$

The deformation gradient is consequently

$$\boldsymbol{F}=\boldsymbol{F}_1\boldsymbol{F}_2=v'f'\mathbf{e}_r\otimes\boldsymbol{E}_1+fg'\mathbf{e}_\theta\otimes\boldsymbol{E}_2+\mathbf{e}_z\otimes\boldsymbol{E}_3 \tag{B5}$$

and $J=v'f'fg'$. Let f and g be selected so that the deformation from $\mathscr{B}_{\mathrm{int}}$ to $\mathscr{B}$ is incompressible, namely

$$f'(\overline{X}_1)f(\overline{X}_1)g'(\overline{X}_2)=1 \tag{B6}$$

then f and g are determined

$$f(\overline{X}_1)=\sqrt{\frac{l_0}{\overline{\theta}}\overline{X}_1+r_i^2},\quad g(\overline{X}_2)=\frac{2\overline{\theta}}{l_0}\overline{X}_2 \tag{B7}$$

DOI: 10.1002/nme

and

$$J = v' \tag{B8}$$

Note that the latter equation implies that J is only a function of r.

The left Cauchy Green deformation tensor is

$$\boldsymbol{B} = (v')^2 \frac{a^2}{r^2} \mathbf{e}_r \otimes \mathbf{e}_r + \frac{r^2}{a^2} \mathbf{e}_\theta \otimes \mathbf{e}_\theta + \mathbf{e}_z \otimes \mathbf{e}_z \tag{B9}$$

where $a = l_0/(2\overline{\theta})$. From Equation (24) the *total* Cauchy stress tensor is

$$\boldsymbol{T} = T_r \mathbf{e}_r \otimes \mathbf{e}_r + T_\theta \mathbf{e}_\theta \otimes \mathbf{e}_\theta + T_z \mathbf{e}_z \otimes \mathbf{e}_z \tag{B10}$$

with

$$T_r = \mathscr{K} \frac{1}{J} (\mathrm{Ln}J - \mathrm{Ln}J_{s-f}) + \mu \frac{1}{J} \left[J^{2/3} \frac{a^2}{r^2} - \frac{1}{3} \left(J^{2/3} \frac{a^2}{r^2} + J^{-1/3} \frac{r^2}{a^2} + J^{-1/3} \right) \right] \tag{B11}$$

$$T_\theta = \mathscr{K} \frac{1}{J} (\mathrm{Ln}J - \mathrm{Ln}J_{s-f}) + \mu \frac{1}{J} \left[J^{-1/3} \frac{r^2}{a^2} - \frac{1}{3} \left(J^{2/3} \frac{a^2}{r^2} + J^{-1/3} \frac{r^2}{a^2} + J^{-1/3} \right) \right] \tag{B12}$$

$$T_z = \mathscr{K} \frac{1}{J} (\mathrm{Ln}J - \mathrm{Ln}J_{s-f}) + \mu \frac{1}{J} \left[J^{-1/3} - \frac{1}{3} \left(J^{2/3} \frac{a^2}{r^2} + J^{-1/3} \frac{r^2}{a^2} + J^{-1/3} \right) \right] \tag{B13}$$

where, from Equations (26) and (27), J_{s-f} is obtained as the solution of the following implicit equation:

$$\frac{\mathrm{Ln}J_{s-f}}{J_{s-f}} = \exp\left(\frac{\mathscr{K}(\mathrm{Ln}J - \mathrm{Ln}J_{s-f})}{(1-n_0)\mathscr{K}_s} \right) \frac{p_w}{\mathscr{K}_s} \tag{B14}$$

Two simple cases can be considered. In the first the pore pressure is null ($p_w = 0$), so $J_{s-f} = 1$. This case represents a particular *drained* condition and can be practically obtained by applying a sufficiently slow loading condition to a permeable porous medium. In this case, the two-phase medium practically behaves like a single-phase medium. The same response would be obtained for a dry porous medium, if air compressibility were negligible.

The second simple case is of a null relative motion between the fluid and solid phases. It can be practically obtained in impermeable porous media submitted to a sufficiently rapid quasi-static deformation, which is why it is usually denoted as an *undrained* condition. In this case, the variation in fluid mass is null (i.e. $\bar{m}_w = 0$), so from Equations (5) and (7), and from the constitutive equation of the pore fluid

$$p_w = -\mathscr{K}_w \mathrm{Ln} \frac{\rho_{w0}}{\rho_w} \tag{B15}$$

the pore pressure amounts to

$$p_w = -\mathscr{K}_w \mathrm{Ln} \left[\frac{1}{n_0} J + \left(1 - \frac{1}{n_0} \right) J_{s-f} \exp\left(\frac{\mathscr{K}(\mathrm{Ln}J - \mathrm{Ln}J_{s-f})}{(1-n_0)\mathscr{K}_s} \right) \right] \tag{B16}$$

From Equations (B14) and (B16), J_{s-f} and p_w can be expressed in terms of J, and are, consequently, only functions of r.

The momentum balance equations expressed in the deformed configuration are as follows:

$$\frac{\partial T_r}{\partial r} + \frac{T_r - T_\theta}{r} = 0, \quad \frac{\partial T_\theta}{\partial \theta} = 0 \tag{B17}$$

the latter one being identically satisfied. Equation $(B17)_1$ is a first-order differential equation of $J(r)$, which can be obtained through the integration of Equation $(B17)_1$ with the boundary condition $T_r(r_i) = 0$, leading to the evaluation of the unknown integration constant.

DOI: 10.1002/nme

Finally the integration of the differential equation (B8), i.e.

$$v'(X_1)=J\left(\sqrt{\frac{l_0}{\overline{\theta}}v(X_1)+r_i^2}\right) \tag{B18}$$

with the boundary condition $v(-h_0/2)=0$ leads to the evaluation of the function $v(X_1)$.

The last equation that remains to be fulfilled is the equality of the volumes in $\mathscr{B}_{\text{int}}$ and $\mathscr{B}$, namely

$$\overline{h}_0 l_0=2\overline{\theta}\int_{r_i}^{r_i+h} r\,\mathrm{d}r=2\overline{\theta}\left(hr_i+\frac{h^2}{2}\right) \tag{B19}$$

which coincides with Equation $(B7)_1$. As a result, once $\overline{\theta}$ has been selected, the unknown values of r_i, $\overline{h}_0$ and h can be obtained by solving the non-linear system of equations consisting of Equation (B19), and the two boundary conditions $T_r(r_i+h)=0$ and $v(h_0/2)=\overline{h}_0$.

The integration of the unknown functions $J(r)$ and $v(X_1)$, and the solution of the non-linear system of equations have been performed numerically using the interpolation functions and the facilities offered by Mathematica.

ACKNOWLEDGEMENTS

Financial support from the University of Trento is gratefully acknowledged. Additionally, R. Denzer acknowledges the financial support from PRIN Grant No. 2007YZ3B24 financed by Italian MIUR.

REFERENCES

1. Loix F, Simoes FMF, Loret B. Articular cartilage with intra and extrafibrillar waters—simulations of mechanical and chemical loadings by the finite element method. *Computer Methods in Applied Mechanics and Engineering* 2008; **197**:4840–4857.
2. Biot MA. A general theory of three-dimensional consolidation. *Journal of Applied Physics* 1941; **12**:155–164.
3. Biot MA. Theory of propagation of elastic waves in a fluid saturated porous solid. *Journal of the Acoustical Society of America* 1956; **28**:168–191.
4. Biot MA. Mechanics of deformation and acoustic propagation in porous media. *Journal of Applied Physics* 1962; **27**:459–467.
5. Biot MA. Generalized theory of acoustic propagation in porous dissipation media. *Journal of the Acoustical Society of America* 1962; **34**:1254–1264.
6. Morland LW. A simple constitutive theory for a fluid-saturated porous solid. *Journal of Geophysical Research* 1972; **77**:890–900.
7. Bowen RM. Theory of mixtures. In *Continuum Physics*, Eringen C (ed.), vol. 3. Academic Press: New York, 1976; 1–127.
8. Bowen RM. Compressible porous media models by use of the theory of mixtures. *International Journal of Engineering Science* 1982; **20**:697–735.
9. Biot MA. Theory of finite deformations of porous solids. *Indiana University Mathematics Journal* 1972; **21**: 597–620.
10. Biot MA. Nonlinear and semilinear rheology of porous media. *Journal of Geophysical Research* 1973; **78**: 4924–4937.
11. Biot MA. Variational Lagrangian thermodynamics of nonisothermal finite strain: mechanics of porous solid and thermomolecular diffusion. *International Journal of Solids and Structures* 1977; **13**:579–597.
12. Coussy O. Thermomechanics of saturated porous solids in finite deformations. *European Journal of Mechanics—A/Solids* 1989; **8**:1–14.
13. Detournay E, Cheng AHD. Foundamentals of poroelasticity. In *Comprehensive Rock Engineering*: *Principles, Practice and Projects. II*: *Analysis and Design Method*, Hudson JA (ed.). Pergamon: New York, 1993; 113–171.
14. Schanz M, Diebels S. A comparative study of Biot's theory and the linear Theory of Porous Media for wave propagation problems. *Acta Mechanica* 2003; **161**:213–235.
15. Garg SK, Nayfeh H, Good AJ. Compressional waves in fluid-saturated elastic porous media. *Journal of Applied Physics* 1974; **45**:1968–1974.
16. Simon BR, Wu JS-S, Zienkiewicz OC, Paul DK. Evaluation of $u-w$ and $u-\pi$ finite element methods for the dynamic response of saturated porous media using one-dimensional models. *International Journal for Numerical and Analytical Methods in Geomechanics* 1986; **10**:461–482.

DOI: 10.1002/nme

17. Simon BR, Wu JS-S, Zienkiewicz OC, Paul DK. Evaluation of higher order, mixed and hermitean finite element procedures for dynamic analysis of saturated porous media using one-dimensional models. *International Journal for Numerical and Analytical Methods in Geomechanics* 1986; **10**:483–499.
18. Gajo A, Mongioví L. An analytical solution for the transient response of saturated linear elastic porous media. *International Journal for Numerical and Analytical Methods in Geomechanics* 1995; **19**:399–413.
19. Schanz M. Poroelastodynamics: linear models, analytical solutions, and numerical methods. *Applied Mechanics Reviews* 2009; **62**(3):52–79.
20. Gaboussi J, Wilson EL. Variational formulation of dynamics of fluid-saturated porous elastic solids. *Proceedings of the ASCE* 1973; EM4, **98**:947–962.
21. Zienkiewicz OC, Shiomi T. Dynamic behaviour of saturated porous media: the generalized Biot formulation and its numerical solution. *International Journal for Numerical and Analytical Methods in Geomechanics* 1984; **8**:71–96.
22. Gajo A, Saetta A, Vitaliani R. Evaluation of three-and two-field finite element methods for the dynamic response of saturated soil. *International Journal for Numerical Methods in Engineering* 1994; **37**:1231–1247.
23. Carter JP, Booker JR, Small JC. The analysis of finite elasto-plastic consolidation. *International Journal for Numerical and Analytical Methods in Geomechanics* 1979; **3**:107–129.
24. Prevost JH. Nonlinear transient phenomena in saturated porous media. *Computer Methods in Applied Mechanics and Engineering* 1982; **20**:3–18.
25. Bennethum LS. Compressibility moduli for porous materials incorporating volume fractions. *Journal of Engineering Mechanics* 2006; **132**:1205–1214.
26. Meroi EA, Schrefler BA, Zienckiewicz OC. Large strain static and dynamic semisaturated soil behaviour. *International Journal for Numerical and Analytical Methods in Geomechanics* 1995; **19**:81–106.
27. Diebels S, Ehlers W. Dynamic analysis of a fully saturated porous medium accounting for geometrical and material non-linearities. *International Journal for Numerical Methods in Engineering* 1996; **39**:81–97.
28. Borja RI, Tamagnini C, Alarcón E. Elastoplastic consolidation at finite strain. Part 2: finite element implementation and numerical examples. *Computer Methods in Applied Mechanics and Engineering* 1998; **159**:103–122.
29. Ehlers W, Eipper G. Finite elastic deformations in liquid-saturated and empty porous solids. *Transport in Porous Media* 1999; **34**:179–191.
30. Ehlers W, Markert B. A linear viscoelastic biphasic model for soft tissues based on the theory of porous media. *Transactions of ASME* 2001; **123**:418–424.
31. Ehlers W, Markert B. A macroscopic finite strain model for cellular polymers. *International Journal of Plasticity* 2003; **19**:961–976.
32. Larsson J, Larsson R. Non-linear analysis of nearly-saturated porous media: theoretical and numerical formulation. *Computer Methods in Applied Mechanics and Engineering* 2002; **191**:3883–3907.
33. Sanavia L, Schrefler BA, Steinmann P. A formulation for an unsaturated porous medium undergoing large inelastic strains. *Computational Mechanics* 2002; **28**:137–151.
34. Li C, Borja RI, Regueiro RA. Dynamics of porous media at finite strains. *Computer Methods in Applied Mechanics and Engineering* 2004; **193**:3837–3870.
35. Chen Z, Steeb H, Diebels S. A EVI-space-time Galerkin method for dynamics at finite deformation in porous media. *Computational Mechanics* 2009; **43**:585–601.
36. Markert B, Heider Y, Ehlers W. Comparison of monolithic and splitting solutions schemes for dynamic porous media problems. *International Journal for Numerical Methods in Engineering* 2010; **83**:1341–1383.
37. Advani SH, Lee TS, Lee JK, Kim CS. Hygrothermomechanical evaluation of porous media under finite deformation. Part I—Finite element formulations. *International Journal for Numerical Methods in Engineering* 1993; **36**:147–160.
38. Gajo A. A general approach to isothermal hyperelastic modelling of saturated porous media at finite strains with compressible constituents. *Proceedings of the Royal Society A* 2010; DOI: 10.1098/rspa.2010.0018.
39. Lewis RW, Schrefler BA. *The Finite Element Method in the Static and Dynamic Deformation and Consolidation of Porous Media* (2nd edn). Wiley: Chichester, England, 1998.
40. Armero F. Formulation and finite element implementation of a multiplicative model of coupled poro-plasticity at finite strains under fully saturated conditions. *Computer Methods in Applied Mechanics and Engineering* 1999; **171**:205–241.
41. Li X, Yao D, Lewis RW. A discontinuous Galerkin finite element method for dynamic wave propagation problems in non-linear solids and saturated porous media. *International Journal for Numerical Methods in Engineering* 2003; **57**:1775–1800.
42. Callari C, Armero F. Analysis and numerical simulation of strong discontinuities in finite strain poroplasticity. *International Journal for Numerical Methods in Engineering* 2004; **193**:2941–2986.
43. Bluhm J, De Boer R. Effective stresses—a clarification. *Archive of Applied Mechanics* 1996; **66**:479–492.
44. Diebels S. On the Influence of the matrix compressibility in two-phase models. *Zeitschrift für Angewandte Mathematik und Mechanik* 2000; **80**:S137–S140.
45. Suklje L. *Reological Aspects of Soil Mechanics*. Wiley: New York, 1969.
46. Bernaud D, Deudé V, Dormieux L, Maghous S, Schmitt DP. Evolution of elastic properties in finite poroplasticity and finite element analysis. *International Journal for Numerical and Analytical Methods in Geomechanics* 2002; **26**:845–871.

47. Larsson R, Wysocki M, Toll S. Process-modeling of composites using two-phase porous media theory. *European Journal of Mechanics—A/Solids* 2004; **23**:15–36.
48. Borja RI. On the mechanical energy and effective stress in saturated and unsaturated porous continua. *International Journal of Solids and Structures* 2006; **43**:1764–1786.
49. Nur A, Byerlee J. An exact effective stress law for elastic deformation of rock with fluids. *Journal of Geophysical Research* 1971; **76**:6414–6419.
50. Johnson GC, Bammann DJ. A discussion of stress rates in finite deformation problems. *International Journal of Solids and Structures* 1984; **20**:725–737.
51. Zienkiewicz OC, Chang CT, Bettess P. Drained, undrained consolidating and dynamic behaviour assumptions in soils. Limits of validity. *Geotechnique* 1980; **30**:385–395.
52. Gajo A. The influence of viscous coupling in the propagation of elastic waves in saturated soil. *Journal of Geotechnical Engineering* (ASCE) 1995; **121**:636–644.
53. Chen Z, Steeb H, Diebels S. A time-discontinuous Galerkin method for the dynamical analysis of porous media. *International Journal for Numerical and Analytical Methods in Geomechanics* 2006; **30**:1113–1134.
54. Prevost JH. Mechanics of continuous porous media. *International Journal of Engineering Science* 1980; **18**: 787–800.
55. Coussy O. *Mechanics of Porous Media*. Wiley: Chichester, 1995.
56. Gurtin ME. *An Introduction to Continuum Mechanics*. Academic Press: San Diego, CA, 1981.
57. Markert B. A constitutive approach to 3-d nonlinear fluid flow through finite deformable porous media. *Transport in Porous Media* 2007; **70**:427–450.
58. Truesdell C, Toupin R. The classical field theories. In *Handbuch der Physik*, Flügge S (ed.), vol. III. Springer: Berlin, 1960.
59. Archie GE. The electrical resistivity log as an aid in determining some reservoir characteristics. *Transactions of AIME* 1942; **146**:54–62.
60. Sen PN, Scala C, Cohen MH. A self-similar model for sedimentary rocks with application to the dielectric constant of fused glass beads. *Geophysics* 1981; **46**:781–795.
61. Gajo A. The effects of inertial coupling in the interpretation of dynamic soil tests. *Géotechnique* 1996; **46**:245–257.
62. Malvern LE. *An Introduction to the Mechanics of a Continuous Medium*. Prentice-Hall: Englewood Cliffs, NJ, 1969.
63. Li X, Liu ZL, Lewis RW, Suzuki K. Mixed finite element method for saturated poroelastic media at large strains. *International Journal for Numerical Methods in Engineering* 2003; **57**:875–898.
64. Zienkiewicz OC, Taylor RL. *The Finite Element Method* (5th edn). Butterworth Heinemann: Oxford, England, 2000.
65. Chen Z, Steeb H, Diebels S. A new hybrid velocity integration method applied to elastic wave propagation. *International Journal for Numerical Methods in Engineering* 2008; **74**:56–79.
66. Li XD, Wiberg NE. Implementation adaptivity of a space-time finite element method for structural dynamics. *Computer Methods in Applied Mechanics and Engineering* 1998; **156**:211–229.
67. Eason G, Fulton J, Sneddon IN. The generation of waves in an infinite elastic solid by variable body forces. *Philosophical Transactions of the Royal Society* 1956; **A248**:575–607.
68. Miehe C. Entropic thermoelasticity at finite strains. Aspects of the formulation and numerical implementation. *Computer Methods in Applied Mechanics and Engineering* 1995; **120**:243–269.
69. Reese S, Govindjee S. Theoretical and numerical aspects in the thermo-viscoelastic material behaviour of rubber-like polymers. *Mechanics of Time-Dependent Materials* 1998; **1**:357–396.
70. Simo JC. Numerical analysis and simulation of plasticity. In *Handbook of Numerical Analysis*, Ciarlet PG, Lions JL (eds), vol. VI. North-Holland: Amsterdam, 1998.
71. Kuhl E, Denzer R, Barth FJ, Steinmann P. Application of the material force method to thermo-hyperelasticity. *Computer Methods in Applied Mechanics and Engineering* 2004; **193**:3303–3325.
72. Green AE, Zerna W. *Theoretical Elasticity* (2nd edn). Oxford University Press: Oxford, 1968.
73. Ogden RW. *Non-Linear Elastic Deformations*. Dover: New York, 1984.

DOI: 10.1002/nme